NOMA-Enabled Multi-Beam Satellite Systems: Joint Optimization to Overcome Offered-Requested Data Mismatches

Anyue Wang, *Graduate Student Member, IEEE*, Lei Lei, *Member, IEEE*, Eva Lagunas, *Senior Member, IEEE*, Ana I. Pérez-Neira, *Fellow, IEEE*, Symeon Chatzinotas, *Senior Member, IEEE*, and Björn Ottersten, *Fellow, IEEE*

***Abstract*—Non-orthogonal multiple access (NOMA) has potentials to improve the performance of multi-beam satellite systems. The performance optimization in satellite-NOMA systems could be different from that in terrestrial-NOMA systems, e.g., considering distinctive channel models, performance metrics, power constraints, and limited flexibility in resource management. In this paper, we adopt a metric, offered capacity to requested traffic ratio (OCTR), to measure the requested-offered data rate mismatch in multi-beam satellite systems. In the considered system, NOMA is applied to mitigate intra-beam interference while precoding is implemented to reduce inter-beam interference. We jointly optimize power, decoding orders, and terminal-timeslot assignment to improve the max-min fairness of OCTR. The problem is inherently difficult due to the presence of combinatorial and non-convex aspects. We first fix the terminal-timeslot assignment, and develop an optimal fast-convergence algorithmic framework based on Perron-Frobenius theory (PF) for the remaining joint power-allocation and decoding-order optimization problem. Under this framework, we propose a heuristic algorithm for the original problem, which iteratively updates the terminal-timeslot assignment and improves the overall OCTR performance. Numerical results show that the proposed algorithm improves the max-min OCTR by 40.2% over orthogonal multiple access (OMA) in average.**

***Index Terms*—Max-min fairness, multi-beam satellite systems, non -orthogonal multiple access (NOMA), offered capacity to requested traffic ratio (OCTR), resource optimization.**

I. Introduction

A MULTI-BEAM satellite system provides wireless services to wide-range areas. On the one hand, traffic distribution is typically asymmetric among beams [1]. On the other hand, satellite capacity is restricted by practical aspects, e.g., payload design, limited flexibility in resource management, and tended to be fixed before launch [2]. The asymmetric traffic and the pre-designed capacity could result in mismatches between requested traffic and offered capacity [3], i.e., hot beams with unmet traffic demand or cold beams with unused capacity [4]. Both cases are undesirable for satellite operators, which motivates the investigation of flexible resource allocation to reduce the mismatches for future multi-beam satellite systems.

A. Related Works: NOMA in Terrestrial and Satellite Systems

In terrestrial systems, non-orthogonal multiple access (NOMA) has demonstrated its superiority, e.g., in throughput, energy, fairness, etc., [5], [6], over orthogonal multiple access (OMA). By performing superposition coding at the transmitter side, more than one terminal's signal can be superimposed with different levels of transmit power and broadcast to co-channel allocated terminals. At the receiver side, successive interference cancellation (SIC) is performed. In this way, NOMA is capable of alleviating co-channel interference, accommodating more terminals, and improving spectral efficiency [6].

The authors in [7]–[10] analyzed the applicability of integrating NOMA to satellite systems. In [7], NOMA was applied in satellite-terrestrial integrated systems to improve capacity and fairness. NOMA was considered in multi-beam satellite systems in [8], [9], where precoding, power allocation, and user grouping schemes were studied to maximize the capacity. In [10], the authors provided an overview for applying NOMA to satellite networks. Under a single-beam scenario, the authors in [11], [12] analyzed outage performance for satellite-NOMA. In [11], a comprehensive study on outage probability, capacity, and energy efficiency for a NOMA-based land mobile satellite network was provided. In [12], the outage performance of a NOMA-based satellite network was investigated in the cases of perfect and imperfect SIC.

In the literature, resource optimization for NOMA-enabled multi-beam satellite systems is studied to a limited extent. First, the study of integration between NOMA and the satellite is limited, e.g., [13], [14], where the satellite is functioned as a supplemental component. In both works, NOMA was applied to the terrestrial systems but not to the satellite component. Second,

Manuscript received July 9, 2020; revised November 1, 2020; accepted December 15, 2020. Date of publication December 25, 2020; date of current version February 12, 2021. This work was supported by the FNR CORE projects ROSETTA (11632107) and FlexSAT (C19/IS/13696663), and in part by the project TERESA (TEC2017-90093-C3-1-R). A part of this work was presented at IEEE International Symposium on Personal, Indoor and Mobile Radio Communications (PIMRC), 2019 [21]. The review of this article was coordinated by Dr. Boya Di. *(Corresponding author: Lei Lei.)*

Anyue Wang, Lei Lei, Eva Lagunas, Symeon Chatzinotas, and Björn Ottersten are with the Interdisciplinary Center for Security, Reliability and Trust, University of Luxembourg, 1855, Luxembourg (e-mail: anyue.wang@uni.lu; lei.lei@uni.lu; eva.lagunas@uni.lu; schatzin@ieee.org; bjorn.ottersten@uni.lu).

Ana I. Pérez-Neira is with the Centre Tecnològic de Telecomunicacions de Catalunya, 08860 Castelldefels, Spain and Universitat Politècnica de Catalunya, 08034 Barcelona, Spain (e-mail: aperez@cttc.es).

Digital Object Identifier 10.1109/TVT.2020.3047453

the previous satellite-NOMA works commonly adopted general terrestrial-oriented metrics, e.g., capacity [7], [8], fairness [7], and outage probability [11], [12]. Nevertheless, practical and featured metrics for multi-beam satellite systems, e.g., mismatches between requested traffic and offered capacity, have not been fully discussed. Third, for NOMA-enabled multi-beam satellite systems, how to derive an appropriate decoding order which is coupling with the beam-power variations, needs to be addressed. The authors in [15] studied power optimization to reduce the traffic-capacity mismatch for NOMA-based multi-beam satellite systems, with adopting a predefined and fixed decoding order, thus simplifying the power allocation. In practical scenarios, decoding orders may change when beam power is adjusted [16]. Therefore, it is important to optimize decoding orders for multi-beam satellite systems since an inappropriate decoding order can result in unsuccessful SIC and thus performance degradation. In this paper, we consider a full frequency reuse system, where inter-beam interference is mitigated via precoding while NOMA is applied to reduce intra-beam interference within a beam.

B. Challenges and Contributions

In general, resource allocation schemes for terrestrial multi-antenna NOMA systems may not be directly applied to multi-beam satellite systems [2], [9]. For instance, terminals with highly correlated channels and large channel-gain difference are favorable to be grouped to mitigate inter-beam and intra-beam interference by precoding and NOMA, respectively [17]–[19]. Such desired terminal groups or pairs can be observed in terrestrial-NOMA systems but might not be easily obtained in satellite scenarios. In addition, channel models, payload design, and on-board limitations could render resource optimization in satellite-NOMA systems more challenging than terrestrial-NOMA systems [20].

In this paper, we focus on how NOMA can help to improve the performance of the practical metric, offered capacity to requested traffic ratio (OCTR), in multi-beam satellite systems. The main contributions are summarized as follows:

- We formulate a max-min resource allocation problem to jointly optimize power allocation, decoding orders, and terminal-timeslot assignment, such that the lowest OCTR among terminals can be maximized. The problem falls into the domain of combinatorial non-convex programming, which brings more performance gain in OCTR but is more challenging compared to our previous work [21].
- Unlike previous studies, we develop a simple approach to circumvent the difficulties in jointly optimizing undetermined optimal decoding order and undetermined rate-function expressions based on the derived theoretical analysis.
- By fixing the terminal-timeslot assignment, we augment the power-tune solution in [21] and propose a Perron-Frobenius theory (PF) based approach to solve the remaining problem, i.e., jointly optimizing power allocation and decoding orders (JOPD). We also provide theoretical results to prove that the approach is with guaranteed fast convergence to the optimum. The fixed terminal-timeslot assignment is determined by grouping the terminals with maximum channel correlation (MaxCC).
- We provide a complete algorithmic solution for the considered joint optimization problem. Under the framework of JOPD, we develop a heuristic algorithm to jointly optimizing power allocation, decoding orders, and terminal-timeslot scheduling (JOPDT), which iteratively updates terminal-timeslot assignment and precoding vectors, and improves the overall OCTR performance. JOPDT aims at providing benchmarks and upper bounds for JOPD.
- The numerical results, firstly, verify the fast convergence of JOPD. Secondly, we show the OCTR performance gain of NOMA over OMA in the two proposed NOMA-based schemes, i.e., JOPD+MaxCC (with lower complexity) and JOPDT (with higher complexity). Thirdly, we compare the performance of the max-min OCTR objective with another widely-used objective. Lastly, we evaluate the OCTR performance in the scenarios with practical consideration, e.g., atmospheric-fading effects and SIC imperfection, to demonstrate the applicability of the proposed algorithms to more practical scenarios.

TABLE I
LIST OF ACRONYMS

Acronyms	Definitions
NOMA	non-orthogonal multiple access
OMA	orthogonal multiple access
SIC	successive interference cancellation
OCTR	offered capacity to requested traffic ratio
PF	Perron-Frobenius theory
JOPD	jointly optimizing power allocation and decoding orders
MaxCC	maximum channel correlation
JOPDT	jointly optimizing power allocation, decoding orders, and terminal-timeslot scheduling
GEO	geostationary earth orbit
MMSE	minimum mean square error
CSI	channel state information
SINR	signal-to-interference-plus-noise ratio
MCMU	monotonic constrained max-min utility
CUF	competitive utility function
MC	monotonic constraint
MIECP	mixed-integer exponential conic programming

The remainder of the paper is organized as follows: Section II introduces the system model of NOMA-enabled multi-beam satellite systems. The max-min optimization problem is formulated in Section III. We propose a PF-based algorithmic framework, JOPD, to solve the problem with the fixed terminal-timeslot scheduling in Section IV. In Section V, the heuristic algorithm JOPDT is put forward to solve the original problem. The simulation settings are displayed and the numerical results are analyzed in Section VI. Section VII concludes the paper.

The notations in this paper are as follows: The operators $[\cdot]^T$ and $[\cdot]^H$ denote the transpose and conjugate transpose operator, respectively. $|\cdot|$ represents the cardinality of a set or the absolute value. $\|\cdot\|$ denotes the Euclidean norm of a vector. $[\cdot]_{i,j}$ represents the element in the i-th row and the j-th column of a matrix.

II. SYSTEM MODEL

A. Multi-Beam Satellite System

We consider the forward-link transmission in a multi-beam satellite system, where a geostationary earth orbit (GEO) satellite is equipped with an array-fed reflector antenna to generate

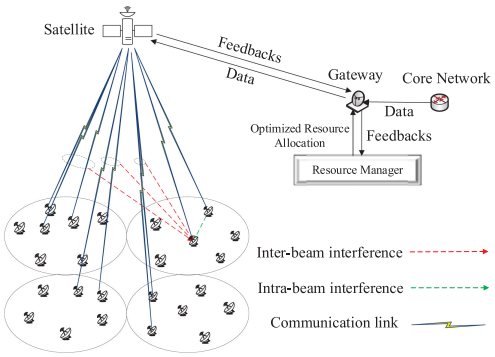

Fig. 1. An illustrative scenario of the NOMA-enabled multi-beam satellite system, where all the beams share the same frequency band.

B spot beams. The satellite provides fixed services to ground terminals. Each terminal is equipped with a single antenna. We denote $\mathcal{B} = \{1, \ldots, B\}$ as the set of the beams. One feed per beam is implemented in the system and the index of a feed is assumed to be consistent with that of the beam it serves. We follow a typical scenario in satellite systems, e.g., [1], [2], [4], [8], as shown in Fig. 1. The motivation is to facilitate our investigation on how NOMA-enabled resource optimization performs in an aggressive frequency-reuse scenario for addressing a practical issue, i.e., to overcome the mismatch effect between requested traffic and offered capacity. The gateway with the co-located resource management unit connects the core network and the satellite payload. The gateway collects terminals' feedbacks, e.g., channel conditions and traffic demand, via the return link. The resource manager is responsible for generating optimized decisions, and the outcome is communicated to the gateway and then to the payload. The satellite plays as a transparent transceiver to relay data from the gateway to ground terminals.

Let $\mathcal{U}_b$ be the set of all the fixed ground terminals located within the service area of the b-th beam. For each scheduling period, K_b terminals from $\mathcal{U}_b$ are selected for transmission. Denote $\mathcal{K}_b = \{1, \ldots, K_b\}$ as the set of the selected terminals in beam b, where $\mathcal{K}_b \subseteq \mathcal{U}_b$. We focus on resource allocation during a scheduling period consisting of C timeslots. Let $\mathcal{C} = \{1, \ldots, C\}$ be the set of the timeslots.

As we consider fixed ground terminals, the channel gains vary over scheduling periods but keep static during a scheduling period. Define $\mathbf{h}_{bk} = [h^1_{bk}, \ldots, h^i_{bk}, \ldots, h^B_{bk}]^T \in \mathbb{C}^{B\times 1}$ as the channel vector of the k-th terminal in beam b at timeslot c. The i-th element of the vector, h^i_{bk}, denotes the channel coefficient from the i-th feed to the k-th terminal in beam b, where $i \in \mathcal{B}$. The channel coefficient can be expressed as $h^i_{bk} = e^{\mathrm{j}\vartheta_{bk}}\sqrt{\frac{G^{\mathrm{Sat}}_{ibk} L_{bk} G^{\mathrm{Rx}}_{bk}}{\kappa T B_W}}$, where G^{Sat}_{ibk} is the transmit antenna gain corresponding to the off-axis angle between the beam center and the terminal. Let L_{bk} denote the free-space propagation loss from the GEO satellite to the k-th terminal in beam b, which is calculated by $L_{bk} = (\frac{v}{4\pi f_{\mathrm{freq}} d_{bk}})^2$, where v, f_{freq}, and d_{bk} represent the propagation speed, the frequency, and the distance between the GEO satellite and the k-th terminal in beam b, respectively. G^{Rx}_{bk} is the receiver antenna gain. $\kappa T B_W$ is the noise distribution, where κ, T, and B_W denote the Boltzmann constant, the receiver noise temperature, and the occupied bandwidth, respectively. $e^{\mathrm{j}\vartheta_{bk}}$ denotes the phase variation due to the long propagation paths to each terminal, where ϑ_{bk} is uniformly distributed between 0 and 2π. The channel model has been widely adopted in the literature, e.g., [8], [22], [23]. By introducing NOMA and precoding to mitigate interference, 1-color frequency-reuse pattern is adopted, where all the beams share the same frequency band [2]. In terms of payload, the on-board payload is equipped with the module of multi-port amplifier (MPA) such that power can be flexibly distributed across different beams.

B. Precoding and NOMA

To alleviate inter-beam interference, we adopt a linear precoding scheme, minimum mean square error (MMSE), which has been widely considered in satellite systems, e.g., [1], [2], [8], [24], [25]. Compared to zero-forcing, maximum-ratio, and dirty-paper coding schemes, MMSE can achieve a good trade-off between high spectral efficiency and low computational complexity [26]. In the system model, we assume that channel state information (CSI) is available at the gateway so that precoding and resource optimization can be performed. In practice, a CSI estimation procedure can be performed first by using pilot-assisted approaches, which is facilitated by the DVB-S2X standard and its superframe structure [27].

Denote $\mathbf{w}_{bc} = [w^1_{bc}, \ldots, w^i_{bc}, \ldots, w^B_{bc}]^T \in \mathbb{C}^{B\times 1}$ as the precoding vector for the b-th beam at timeslot c. The i-th element of the vector, w^i_{bc}, represents the precoding coefficient of the i-th feed for the b-th beam, where $i \in \mathcal{B}$. The received signal can be expressed as:

$$y_{bkc} = \underbrace{\mathbf{h}^H_{bk}\mathbf{w}_{bc}\sqrt{p_{bkc}}s_{bkc}}_{\text{desired signal}} + \underbrace{\sum_{l\in\mathcal{K}_b\setminus\{k\}} \mathbf{h}^H_{bk}\mathbf{w}_{bc}\sqrt{p_{blc}}s_{blc}}_{\text{intra-beam interference}} + \underbrace{\sum_{b'\in\mathcal{B}\setminus\{b\}}\sum_{j\in\mathcal{K}_{b'}} \mathbf{h}^H_{bk}\mathbf{w}_{b'c}\sqrt{p_{b'jc}}s_{b'jc}}_{\text{inter-beam interference}} + \underbrace{n_{bkc}}_{\text{noise}}, \quad (1)$$

where s_{bkc}, p_{bkc}, and $n_{bkc} \sim \mathcal{CN}(0, \sigma^2)$ are the signal with unit power, power scaling factor, and the complex circular symmetric independent identically distributed additive white gaussian noise with zero mean and variance σ^2, respectively. The transmit power of the b-th beam (or feed) is $\rho_{bc}\sum_{k\in\mathcal{K}_b} p_{bkc}$, $\forall c \in \mathcal{C}$, where $\rho_{bc} = [\sum_{i\in\mathcal{B}} \mathbf{w}_{ic}\mathbf{w}^H_{ic}]_{b,b}$ denotes the power radiated by the b-th feed for precoding [22].

To implement MMSE, we construct $\mathbf{H} \in \mathbb{C}^{B\times B}$ as the channel matrix, where the b-th row represents the channel vector of the terminal with $\max_{k\in\mathcal{K}_b} \|\mathbf{h}_{bk}\|$ [19]. The precoding matrix reads,

$$\mathbf{W} = \beta\mathbf{H}^H(\mathbf{H}\mathbf{H}^H + \sigma^2\mathbf{I}_B)^{-1}, \quad (2)$$

where $\mathbf{I}_B$ is the identity matrix with the dimension B by B. β is a scaling factor to normalize the precoding matrix as $[\mathbf{W}\mathbf{W}^H]_{b,b} \le 1$, $\forall b \in \mathcal{B}$. The scaling factor can be determined as $\beta^2 = \frac{1}{\max\{\mathrm{diag}((\mathbf{H}^H\mathbf{H})^{-1})\}}$. Note that the regularization factor before $\mathbf{I}$ is fixed to σ^2 in this paper.

Within a beam, NOMA is applied to mitigate intra-beam interference among terminals. The signal-to-interference-plus-noise

ratio (SINR) γ_{bkc} is expressed as,

$$\gamma_{bkc} = \frac{|\mathbf{h}_{bk}^H \mathbf{w}_{bc}|^2 p_{bkc}}{\sum\limits_{l \in \mathcal{K}_b \setminus \{k\}} \phi_{bklc} |\mathbf{h}_{bk}^H \mathbf{w}_{bc}|^2 p_{blc} + \sum\limits_{b' \in \mathcal{B} \setminus \{b\}} |\mathbf{h}_{bk}^H \mathbf{w}_{b'c}|^2 \sum\limits_{j \in \mathcal{K}_{b'}} p_{b'jc} + \sigma^2}, \tag{3}$$

where $\phi_{bklc} \in \{0, 1\}$ indicates decoding order, where $k \neq l$. Let g_{bkc} denote the ratio between channel gain and inter-beam interference plus noise,

$$g_{bkc} = \frac{|\mathbf{h}_{bk}^H \mathbf{w}_{bc}|^2}{\sum\limits_{b' \in \mathcal{B} \setminus \{b\}} |\mathbf{h}_{bk}^H \mathbf{w}_{b'c}|^2 \sum\limits_{j \in \mathcal{K}_{b'}} p_{b'jc} + \sigma^2}. \tag{4}$$

In the system model, we adopt a descending order of g_{bkc} as the decoding order in SIC, which is a proper decoding order and widely used in the literature for NOMA, e.g., [6], [16], [17], [21], [28]. By the definition, $g_{bkc} > g_{blc}$ means that terminal k decodes the signal of l before decoding its own signal. Otherwise, terminal k treats l's signal as noise when $g_{bkc} < g_{blc}$.

To ease the presentation, we assume the decoding order is consistent with the terminal index, i.e., $g_{b1c} \geq g_{b2c} \geq \cdots \geq g_{bK_bc}$, unless otherwise stated.

The throughput of terminal k in beam b at timeslot c is,

$$R_{bkc} = B_W \log(1 + \gamma_{bkc}). \tag{5}$$

Hence the offered capacity of that terminal is derived as,

$$R_{bk} = \sum_{c \in \mathcal{C}} R_{bkc}. \tag{6}$$

We remark that, in this paper, we assume perfect SIC (as well as CSI) to explore an upper-bound performance of NOMA over OMA. The performance can be served as benchmarks for the cases with various imperfections. In practice, there are a set of approaches being developed, and can be applied to facilitate successful SIC. For instance, one can group terminals with large channel-gain difference and significant power disparity such that the terminals are able to distinguish the intended signal and more likely to perform successful SIC [29]. In addition, some advanced techniques, e.g., soft-in soft-out decoding [30] and multi-branch SIC [31], can help to alleviate the performance degradation caused by imperfect SIC, and keep the error ratio of imperfect SIC at low levels.

III. Problem Formulation

We formulate a max-min fairness problem to improve the OCTR performance by power, decoding-order, and terminal-timeslot optimization. We define the variables and formulate the max-min fairness problem $\mathcal{P}_0$ as follows:

$p_{bkc} \geq 0$, allocated power for terminal k in beam b at timeslot c,

$$\phi_{bklc} = \begin{cases} 0, & \text{in beam } b, \text{terminal } k \text{ decodes } l'\text{s signal at} \\ & \text{timeslot } c \text{ before decoding its own signal,} \\ 1, & \text{terminal } k \text{ does not decode } l'\text{s signal and} \\ & \text{treat it as noise,} \end{cases}$$

$$\alpha_{bkc} = \begin{cases} 1, & \text{terminal } k \text{ in beam } b \text{ is scheduled to time-} \\ & \text{slot } c, \\ 0, & \text{otherwise,} \end{cases}$$

$$\mathcal{P}_0 : \max_{p_{bkc}, \phi_{bklc}, \alpha_{bkc}} \min_{b \in \mathcal{B}, k \in \mathcal{K}_b} \frac{R_{bk}}{D_{bk}} \tag{7a}$$

$$\text{s.t.} \sum_{b \in \mathcal{B}} \rho_{bc} \sum_{k \in \mathcal{K}_b} p_{bkc} \leq P_{tot}, \forall c \in \mathcal{C}, \tag{7b}$$

$$\rho_{bc} \sum_{k \in \mathcal{K}_b} p_{bkc} \leq P_{b,\max}, \forall b \in \mathcal{B}, \forall c \in \mathcal{C}, \tag{7c}$$

$$\rho_{bc} \sum_{k \in \mathcal{K}_b} p_{bkc} = \rho_{bc'} \sum_{k \in \mathcal{K}_b} p_{bkc'}, \quad \forall b \in \mathcal{B}, \forall c, c' \in \mathcal{C}, c \neq c', \tag{7d}$$

$$\sum_{k \in \mathcal{K}_b} \alpha_{bkc} \leq \bar{K}, \forall b \in \mathcal{B}, \forall c \in \mathcal{C}, \tag{7e}$$

$$\sum_{c \in \mathcal{C}} \alpha_{bkc} = 1, \forall b \in \mathcal{B}, \forall k \in \mathcal{K}_b, \tag{7f}$$

$$p_{bkc} \leq \hat{P} \alpha_{bkc}, \forall b \in \mathcal{B}, \forall c \in \mathcal{C}, \forall k \in \mathcal{K}_b, \tag{7g}$$

$$g_{blc} - g_{bkc} \leq A \phi_{bklc}, \quad \forall b \in \mathcal{B}, \forall c \in \mathcal{C}, \forall k, l \in \mathcal{K}_b, k \neq l, \tag{7h}$$

$$\phi_{bklc} + \phi_{blkc} = 1, \quad \forall b \in \mathcal{B}, \forall c \in \mathcal{C}, \forall k, l \in \mathcal{K}_b, k \neq l. \tag{7i}$$

In the objective, we focus on the OCTR improvement and fairness enhancement at the terminal level [23]. The OCTR metric for terminal k in beam b is defined as $\frac{R_{bk}}{D_{bk}}$, where R_{bk} and D_{bk} are the offered capacity and requested traffic demand, respectively. The optimization task is to maximize the worst OCTR among terminals in $\mathcal{K}_b$, such that the mismatch and the fairness issues can be addressed. In (7b), the total power is less than a budget P_{tot}, due to the limited on-board power supply. Constraints (7c) state that the allocated power for each beam should be restricted by the power constraint, $P_{b,\max}$. Constraints (7d) denote that, the power allocated to each beam is identical across timeslots, considering the practical issues in waveform design, dynamic range of the signal, and non-linearities of the amplifier [2], [20], [32]. For each beam, the number of terminals simultaneously accessing the same timeslot is no more than $\bar{K}$ in (7e). In (7f), each terminal is limited to be scheduled once during a scheduling period to avoid imbalanced timeslot assignment among terminals, which is important for serving a large number of terminals. Constraints (7g) connect two sets of variables, p_{bkc} and α_{bkc}, where $\hat{P}$ is no smaller than the maximal p_{bkc}, e.g., $\hat{P} = P_{tot}$. If $\alpha_{bkc} = 0$, p_{bkc} is zero. If $\alpha_{bkc} = 1$, $\hat{P} \geq p_{bkc} > 0$ since the option $\alpha_{bkc} = 1$ and $p_{bkc} = 0$ is clearly not optimal, thus will be excluded from the optimum. Constraints (7h) and (7i) confine variables ϕ_{bklc} to perform SIC by the descending order defined in (4), where A is no smaller than the maximum value of g_{bkc}. If $g_{bkc} > g_{blc}$, $\phi_{bklc} = 0$ which means that terminal k decodes the signal of l before decoding its own signal, and terminal l treats k's signals as noise. If $\phi_{bklc} = 1$, it implies $g_{bkc} < g_{blc}$, then terminal k does not decode l's signal and treat it as noise. Note

that due to the constraints $\phi_{bklc} + \phi_{blkc} = 1$ in (7i), $\phi_{bklc} = 1$ also implies $\phi_{blkc} = 0$ and $g_{blc} > g_{bkc}$ in the mean time.

$\mathcal{P}_0$ is a mixed-integer non-convex programming due to the binary variables, α_{bkc} and ϕ_{bklc}, and the non-convexity of R_{bkc}. Solving mixed-integer non-convex programming is in general challenging. A typical way to address a max-min problem is to check whether it can be reformulated as a monotonic constrained max-min utility (MCMU) problem, where the objective functions and constraints are competitive utility functions (CUFs) and monotonic constraints (MCs), respectively [33]. If yes, PF can be applied with fast convergence. The general MCMU is expressed as:

$$\mathcal{P}_{PF}: \max_{\mathbf{Q}} \quad \min_{j=1,\ldots,J} \quad f_j(\mathbf{Q}) \tag{8a}$$

$$\text{s.t.} \quad F_m(\mathbf{Q}) \leq \bar{F}_m, m = 1, \ldots, M. \tag{8b}$$

In $\mathcal{P}_{PF}$, $\mathbf{Q} = [Q_1, \ldots, Q_j, \ldots, Q_J]$ is the vector collecting all the Q-variables. $f_j(\mathbf{Q})$ represents the objective function. $F_m(\mathbf{Q})$ and $\bar{F}_m$ are the constraint functions and upper-bound parameters, respectively. The properties of CUF and MC are presented in Definition 1 and Definition 2, respectively.

Definition 1: The objective function $f_j(\mathbf{Q})$ in $\mathcal{P}_{PF}$ is CUF if the following properties are satisfied:

- *Positivity:* $f_j(\mathbf{Q}) > 0$ *if* $\mathbf{Q} \succ \mathbf{0}$*;* $f_j(\mathbf{Q}) = 0$ *if and only if* $\mathbf{Q} = \mathbf{0}$.
- *Competitiveness:* $f_j(\mathbf{Q})$ *strictly monotonically increases in* Q_j *but decreases in* $Q_{j'}$*, where* $j' \neq j$.
- *Directional Monotonicity: For* $\zeta > 1$ *and* $\mathbf{Q} \succ \mathbf{0}$, $f_j(\zeta\mathbf{Q}) > f_j(\mathbf{Q})$.

Definition 2: The constraints, $F_m(\mathbf{Q}) \leq \bar{F}_m$, $\forall m = 1, \ldots, M$, are MCs if the following properties are satisfied:

- *Strict Monotonicity:* $F_m(\mathbf{Q}_1) > F_m(\mathbf{Q}_2)$ *if* $\mathbf{Q}_1 \succ \mathbf{Q}_2$, $\forall m$.
- *Validity: If* $\mathbf{Q} \succ \mathbf{0}$, $\exists \zeta > 0$ *such that* $F_m(\zeta\mathbf{Q}) \geq \bar{F}_m$ *for some* m.

MCMU and PF may not be directly applied to solve $\mathcal{P}_0$ due to the following reasons:

- The solutions for MCMU (e.g., [33]–[35]) are derived for a specific scenario, e.g., one terminal per cell or per beam. When the scenario of multiple users per beam, along with undetermined decoding orders and binary variables, is considered in this paper, the satisfiability of Definition 1 and Definition 2 no longer holds for original $\mathcal{P}_0$.
- In $\mathcal{P}_0$, determining decoding orders is coupled with beam power allocation. Optimizing beam power could result in changes of decoding orders. As a consequence, the function of R_{bk} in $\mathcal{P}_0$ becomes undetermined (corresponding to the objective function in $\mathcal{P}_{PF}$), which is an obstacle in analyzing the applicability of MCMU and PF.
- Precoding vectors are decided based on the terminal-timeslot assignment. The coupling between precoding vectors and terminal-timeslot assignment could result in undetermined $|\mathbf{h}_{bk}^H \mathbf{w}_{bc}|^2$ in the objective function (7a) while optimizing α_{bkc}.

To solve $\mathcal{P}_0$, the following issues should be tackled. First, the applicability of MCMU and PF for different special cases of $\mathcal{P}_0$ should be analyzed. Second, the challenges to deal with the combinatorial and non-convex components in $\mathcal{P}_0$ need to be addressed. Towards these ends, we first discuss the optimization of power allocation and decoding orders with the fixed terminal-timeslot assignment. Then we focus on solving the whole joint optimization problem.

IV. Optimal Joint Optimization of Power Allocation and Decoding Orders

With fixed α_{bkc} in $\mathcal{P}_0$, we formulate the remaining power and decoding-order optimization problem in $\mathcal{P}_1$.

$$\mathcal{P}_1: \max_{p_{bkc}>0, \phi_{bklc}} \quad \min_{b\in\mathcal{B}, k\in\mathcal{K}_b} \quad \frac{R_{bk}}{D_{bk}} \tag{9a}$$

$$\text{s.t.} \quad (7\text{b}), (7\text{c}), (7\text{d}), (7\text{h}), (7\text{i}). \tag{9b}$$

Note that prior to optimization, we have pre-processed p_{bkc} according to the fixed variables α_{bkc}. That is, only positive p-variables, i.e., $p_{bkc} > 0$ (resulted by $\alpha_{bkc} = 1$), retain in $\mathcal{P}_1$ and to be optimized. $\mathcal{P}_1$ is complicated due to the coupled power and decoding-order optimization. From $\mathcal{P}_1$, we can observe that if the decoding orders can be determined by temporarily fixing the beam power, the remaining power allocation problem resembles P_{PF}. This enables us to take advantages of the PF method in fast convergence and optimality guarantee. In this section, we first discuss the strategy of fixing the terminal-timeslot assignment. Next, we discuss the solution of $\mathcal{P}_1$, and the applicability of MCMU and PF.

A. Terminal-Timeslot Scheduling

Terminal-timeslot scheduling or terminal grouping is significant for NOMA and precoding. In the literature, the grouping strategies are either optimal or suboptimal. The former is to find the optimal terminal groups but with prohibitively computational complexity, e.g., an optimal scheme for joint precoding and terminal-subcarrier assignment in [36]. For the latter, some heuristic approaches are developed for terrestrial-NOMA systems but might not be directly applied to satellite NOMA. For example, the strategy of grouping terminals with highly correlated channels and large channel gain difference is widely used in terrestrial-NOMA systems [17]–[19]. However, in satellite systems, neighboring terminals may have highly correlated channels but small channel gain difference [9], whereas terminals far away from each other may have non-correlated channels.

Considering the trade-off between interference reduction and computational complexity, we apply MaxCC strategy to select terminals with the largest correlation [22]. The reason behind this strategy is that the precoder should be able to mitigate inter-beam interference more effectively whenever the terminals grouped within the same beam have highly correlated channel vectors. The procedure is summarized in the following. In a timeslot, we select one terminal, say k', randomly from $\mathcal{U}_b$. Then we calculate its correlation factors (or cosine similarity metric) with all the other terminals, i.e., $\theta = \frac{|\mathbf{h}_{bk'}^H \mathbf{h}_{bj}|}{\|\mathbf{h}_{bk'}\| \|\mathbf{h}_{bj}\|}$ [8], where $j \in \mathcal{U}_b \setminus \{k'\}$. The terminal with the largest θ is scheduled with k' to the same timeslot. The selected terminals are deleted

from $\mathcal{U}_b$ and added to $\mathcal{K}_b$. The above procedure is performed for each timeslot one by one until all the timeslots are processed or $\mathcal{U}_b$ becomes empty.

B. Terminal Power Optimization With Fixed Beam Power

We define $\mathbf{P} = [P_1, \ldots, P_b, \ldots, P_B]$ as the vector collecting all the beam power. With fixed α_{bkc} and temporarily fixed $\mathbf{P}$, the terminal power allocation is independent among beams. Thus $\mathcal{P}_1$ can be decomposed to B subproblems. The b-th subproblem, $\mathcal{P}_1(b)$, corresponds to the terminal power optimization in beam b. Let $\bar{\mathbf{P}}_b$ collect all the beam power except the b-th beam's power, i.e., $\bar{\mathbf{P}}_b = [P_1, \ldots, P_{b-1}, P_{b+1}, \ldots, P_B]$. In (4), g_{bkc} can be considered as a function of $\bar{\mathbf{P}}_b$, which is defined as,

$$g_{bkc} = \hat{f}_{bkc}(\bar{\mathbf{P}}_b). \tag{10}$$

The decoding order variables ϕ_{bklc} are determined when $\mathbf{P}$ is fixed. Thus, constraints (7h) and (7i) do not apply in $\mathcal{P}_1(b)$.

$$\mathcal{P}_1(b): \max_{p_{bkc}} \min_{k\in\mathcal{K}_b} \frac{R_{bk}}{D_{bk}} \tag{11a}$$

$$\text{s.t.} \quad \rho_{bc} \sum_{k\in\mathcal{K}_b} p_{bkc} = P_b, \forall c \in \mathcal{C}, \tag{11b}$$

where (7d) is equivalently converted to (11b) and denotes that the sum of terminals' power in each beam across timeslots is equal to the beam power. By introducing an auxiliary variable t_b, $\mathcal{P}_1(b)$ can be equivalently transformed to a maximization problem:

$$\mathcal{P}_1(b): \max_{p_{bkc}, t_b} \quad t_b \tag{12a}$$

$$\text{s.t.} \quad (11b), \quad t_b D_{bk} - R_{bk} \le 0, \forall k \in \mathcal{K}_b. \tag{12b}$$

To better reveal the convexity of $\mathcal{P}_1(b)$, we express p_{bkc} by a function of R_{bkc} based on (5) [16]. Then the power variables p_{b1c},..., p_{bK_bc} read, $p_{b1c} = \frac{e^{\frac{R_{b1c}}{B_W}}-1}{g_{b1c}}$, $p_{b2c} = \frac{e^{\frac{R_{b2c}}{B_W}}-1}{g_{b2c}}(g_{b2c}p_{b1c} + 1)$,..., $p_{bK_bc} = \frac{e^{\frac{R_{bK_bc}}{B_W}}-1}{g_{bK_bc}}(g_{bK_bc}\sum_{j=1}^{K_b-1} p_{bjc} + 1)$. The constraints in (11b) can be equivalently written as:

$$\sum_{k=1}^{K_b}\left(\frac{1}{g_{bkc}} - \frac{1}{g_{b(k-1)c}}\right) e^{\sum_{j\ge k}\frac{R_{bjc}}{B_W}} - \frac{1}{g_{bK_bc}} = \frac{P_b}{\rho_{bc}}, \forall c \in \mathcal{C}, \tag{13}$$

where $\frac{1}{g_{b0c}} = 0$. Then $\mathcal{P}_1(b)$ is equivalently converted to $\mathcal{P}_2(b)$ by treating R_{bkc} as variables:

$$\mathcal{P}_2(b): \max_{R_{bkc}, t_b} \quad t_b \tag{14a}$$

$$\text{s.t.} \quad (13), (12\text{b}). \tag{14b}$$

Note that constraints (13) are not affine. We further relax the equality constraints in (13) to inequality in (15), leading to a convex exponential-cone format,

$$\sum_{k=1}^{K_b}\left(\frac{1}{g_{bkc}} - \frac{1}{g_{b(k-1)c}}\right) e^{\sum_{j\ge k}\frac{R_{bjc}}{B_W}} - \frac{1}{g_{bK_bc}} \le \frac{P_b}{\rho_{bc}}, \forall c \in \mathcal{C}. \tag{15}$$

We then conclude the equivalence between (13) and (15) at the optimum, thus concluding the convexity of $\mathcal{P}_2(b)$ and $\mathcal{P}_1(b)$.

Proposition 1: The optimum of $\mathcal{P}_2(b)$, i.e., t_b^*, which is located on timeslot c^*, can be obtained by the following equation:

$$\sum_{k=1}^{K_b}\left(\frac{1}{g_{bkc^*}} - \frac{1}{g_{b(k-1)c^*}}\right) e^{\sum_{j\ge k}\frac{t_b^* D_{bj}}{B_W}} - \frac{1}{g_{bK_bc^*}} = \frac{P_b}{\rho_{bc^*}}. \tag{16}$$

Proof: Please refer to Appendix A. ■

Proposition 1 establishes the equivalence between (13) and (15) at the optimum. The convexity of $\mathcal{P}_1(b)$ and $\mathcal{P}_2(b)$ is concluded. We define a function $t_b^* = f_b(\mathbf{P})$ in an inexplicit way in (16) by moving t_b^* to the left side of the equality and the remaining to the right, where $f_b(\mathbf{P})$ denotes the function of the optimal OCTR of beam b when beam power is $\mathbf{P}$.

C. Beam Power Optimization

Given $\mathbf{P}$, the optimal power allocation among terminals can be obtained from Karush-Kuhn-Tucker (KKT) conditions. Next, we optimize the beam power allocation. The problem is formulated in $\mathcal{P}_3$,

$$\mathcal{P}_3: \max_{\mathbf{P}} \min_{b\in\mathcal{B}} \quad f_b(\mathbf{P}) \tag{17a}$$

$$\text{s.t.} \quad \sum_{b\in\mathcal{B}} P_b \le P_{tot}, \tag{17b}$$

$$P_b \le P_{b,\max}, \forall b \in \mathcal{B}, \tag{17c}$$

where the objective $f_b(\mathbf{P})$ is the function of the optimal OCTR of the b-th beam with $\mathbf{P}$ and can be equivalently converted from (16). The expression of $f_b(\mathbf{P})$ depends on $\mathbf{P}$ and the decoding order. Next, we prove $\mathcal{P}_3$ is an MCMU. Constraints (17b) and (17c) are linear, which satisfy the MC conditions. The CUF conditions of $f_b(\mathbf{P})$ are analyzed in Lemma 1 and Lemma 2.

Lemma 1: The objective function $f_b(\mathbf{P})$ in $\mathcal{P}_3$ is a CUF for any decoding orders.

Proof: Please refer to Appendix B. ■

Based on Lemma 1, we can develop PF-based algorithm to converge if the decoding order remains under the power adjustment. However, the expression of $f_b(\mathbf{P})$ typically changes since the adjustment of $\mathbf{P}$ can result in new decoding orders. As a consequence, it is not straightforward to observe the satisfiability of CUF and the convergence when $f_b(\mathbf{P})$ varies. Next, we conclude that the objective function in $\mathcal{P}_3$ is a CUF even if the decoding order changes.

Lemma 2: $f_b(\mathbf{P})$ in $\mathcal{P}_3$ remains a CUF even if the decoding order changes.

Proof: Please refer to Appendix C. ■

Based on Lemma 1 and Lemma 2, the objective function in $\mathcal{P}_3$ is a CUF. Constraints (17b) and (17c) are linear and thus satisfy the MC conditions, which concludes $\mathcal{P}_3$ is an MCMU.

D. Fast-Convergence Approach Based on PF for Joint Power and Decoding-Order Optimization

$\mathcal{P}_3$ is an MCMU where the objective function is CUF and the constraints are MCs. We propose an iterative algorithm based on PF, i.e., JOPD, in Algorithm 1 to solve $\mathcal{P}_3$. Let $\mathbf{P}^{(n)}$, $P_b^{(n)}$ and

Algorithm 1: JOPD.

Input:
Initial beam power, $\mathbf{P}^{(0)}$; iteration index: $n = 0$; maximum number of iterations, $N_{\max}$; precision: $\xi_1 > 0$.

1: **repeat**
2: **for** $b = 1, \ldots, B$ **do**
3: Update and sort g_{bkc} with $\mathbf{P}^{(n)}$.
4: Determine decoding order ϕ_{bklc} based on the descending order of g_{bkc}.
5: Calculate $t_b^{*(n)} = f_b(\mathbf{P}^{(n)})$ by (16).
6: Update $\mathbf{P}$ by $P_b = \frac{P_b^{(n)}}{t_b^{*(n)}}$.
7: **end for**
8: Calculate $\epsilon = \max\{\frac{P_b}{P_{b,\max}}, \forall b \in \mathcal{B}; \sum_{b\in\mathcal{B}} \frac{P_b}{P_{tot}}\}$.
9: Update $\mathbf{P}^{(n+1)} = \frac{\mathbf{P}}{\epsilon}$, $n = n + 1$.
10: **until** $n > N_{\max}$ or $|t_b^{*(n+1)} - t_b^{*(n)}| < \xi_1$
11: Calculate p_{bkc} based on $\mathbf{P}^{(n)}$.

Output:
t_b^*, p_{bkc}.

$t_b^{*(n)}$ represent the values of $\mathbf{P}$, P_b, and t_b^* at the n-th iteration, respectively. For each iteration (line 3 to line 6), decoding orders are updated according to the descending order of g_{bkc} in line 3 and line 4. Then the optimal OCTR of each beam is calculated in line 5. Beam power is adjusted inversely proportional to the value of t_b^* in line 6 [33], which suggests that power for the beams with larger t_b^* will be reduced in the next iteration, and more power is allocated to the beams with worse OCTR. In line 8, we introduce a factor ϵ to confine beam power in the domain of (17b) and (17c). The iteration breaks if either n exceeds the maximum number of iterations, $N_{\max}$, or $|t_b^{*(n+1)} - t_b^{*(n)}|$ is smaller than the tolerance ξ_1. The convergence and optimality of JOPD are concluded in Theorem 1.

Theorem 1: With any initial vector $\mathbf{P}$, JOPD converges geometrically fast to the optimum of $\mathcal{P}_3$.

Proof: Please refer to Appendix C. ■

In JOPD, the complexity of each iteration (line 3 to line 6) is mainly from sorting g_{bkc} in line 3 and deriving $t_b^{*(n)}$ by solving (16) in line 5. Sorting can be achieved by typical methods, e.g., heapsort [37]. The computational complexity of sorting g_{bkc} in beam b for K_b users is $\mathcal{O}(K_b \log(K_b))$ [37]. The complexity of solving the nonlinear equation in (16) with $t_b^{*(n)}$ bounded by [0,1] and tolerance ε_1 is $\mathcal{O}(-\log(\varepsilon_1))$ [38], where $0 < \varepsilon_1 < 1$. Deriving $t_b^{*(n)}$ for each beam in (16) can dominate the complexity when the pre-defined ε_1 is small enough. On the other hand, sorting could be with higher complexity when ε_1 is large. Thus, the complexity of each iteration is $\mathcal{O}(\max\{K_b \log(K_b), -\log(\varepsilon_1)\})$. With maximum $N_{\max}B$ iterations, the complexity of JOPD is $\mathcal{O}(N_{\max}B \max\{K_b \log(K_b), -\log(\varepsilon_1)\})$. Overall, the convergence is geometrically fast if there exist $0 < \varpi < 1$ and a constant $\Pi > 0$ such that $\|P_b^{(n)} - P_b^*\| \leq \Pi\varpi^n$ for all n [33], where P_b^* denotes the optimal beam power.

Next, in Corollary 1, we conclude that although the optimal beam power, coupling with decoding orders, in $\mathcal{P}_1$ is challenging to be directly obtained, the optimum of $\mathcal{P}_1$, in fact, can be achieved by solving a simple problem, i.e., $\mathcal{P}_3$.

Corollary 1: The optimum of $\mathcal{P}_1$ is equal to that of $\mathcal{P}_3$.

The reasons can be explained as follows. $\mathcal{P}_1$ and $\mathcal{P}_3$ solves de facto the same problem, i.e., with the fixed α-variables then obtain the max-min OCTR along with the optimal beam and terminal power allocation since in $\mathcal{P}_3$, when $\mathbf{P}$ is known, p_{bkc} is also known. Theorem 1 indicates that, under the same α_{bkc}, no better beam power allocation than $\mathbf{P}^*$ can be found. Thus $\mathbf{P}^*$ is optimal for $\mathcal{P}_1$ and $\mathcal{P}_3$. Given $\mathbf{P}^*$ to $\mathcal{P}_1$, the resulting max-min OCTR and terminal power allocation are therefore optimal, and thus the conclusion.

The difference between $\mathcal{P}_1$ and $\mathcal{P}_3$ is that, in $\mathcal{P}_1$, one has to deal with the issue of unconfirmed convergence and undetermined optimal R_{bk} expressions due to the decoding-order variations and the undetermined optimal decoding order. In $\mathcal{P}_3$, we circumvent these difficulties by using the established analytical results in this section. By solving $\mathcal{P}_3$ via Algorithm 1, we update beam power associated with decoding order successively, instead of obtaining the optimum directly. Guaranteed by Lemma 1, Lemma 2, and Theorem 1, this simple power-adjustment approach eventually leads to the optimal beam power and optimal decoding order for the given α-variables.

V. Heuristic Algorithm for Joint Power, Decoding-Order, and Timeslot Optimization

JOPD is limited by the one-off terminal-timeslot assignment. Based on the framework of JOPD and taking its fast-convergence advantages, we design a heuristic approach, JOPDT, to iteratively update timeslot-terminal assignment and improve the overall performance. The procedure of the heuristic approach is presented in Algorithm 2.

Line 3 to line 12 present the process of implementing the JOPD framework. In line 2 and line 5, precoding vectors and decoding orders are updated based on the terminal-timeslot assignment and beam power allocation, respectively. In line 7, a joint power-allocation, decoding-order, and terminal-timeslot optimization problem is solved. The problem is constructed as follows. Analogous to JOPD, by fixing $\mathbf{P}$, $\mathcal{P}_0$ is decomposed into B subproblems, each of which represents the optimization of terminals' power allocation and terminal-timeslot assignment in the beam. The b-th subproblem is expressed as,

$$\mathcal{P}_4(b): \max_{p_{bkc},\alpha_{bkc}} \min_{k\in\mathcal{K}_b} \frac{R_{bk}}{D_{bk}} \tag{18a}$$

$$\text{s.t. } \rho_{bc} \sum_{k\in\mathcal{K}_b} p_{bkc} = \rho_{bc'} \sum_{k\in\mathcal{K}_b} p_{bkc'}, \quad \forall c, c' \in \mathcal{C}, c \neq c', \tag{18b}$$

$$\sum_{k\in\mathcal{K}_b} \alpha_{bkc} \leq \bar{K}, \forall c \in \mathcal{C}, \tag{18c}$$

$$\sum_{c\in\mathcal{C}} \alpha_{bkc} = 1, \forall k \in \mathcal{K}_b, \tag{18d}$$

Algorithm 2: JOPDT.

Input:
Initial beam power, $\mathbf{P}^{(0)}$; iteration index in the JOPD framework, $n = 0$; iteration index, $\bar{n} = 0$; maximum iteration in the JOPD framework, $N_{\max}$; maximum iteration, $\bar{N}_{\max}$; initial terminal-timeslot assignment, $\boldsymbol{\alpha}_b^{(0)}, \forall b \in \mathcal{B}$; precision: $\xi_2 > 0$.

1: **repeat**
2: Update precoding vectors $\mathbf{w}_{bc}$ based on $\boldsymbol{\alpha}_b^{(\bar{n})}$.
3: **repeat**
4: **for** $b = 1, \ldots, B$ **do**
5: Update and sort g_{bkc} with $\mathbf{P}^{(n)}$.
6: Decide decoding orders ϕ_{bklc} based on the descending orders of g_{bkc}.
7: Solve $\mathcal{P}_5(b)$ and obtain $\bar{t}_b^{*(n)}$ with $\mathbf{P}^{(n)}$.
8: Update $\mathbf{P}$ by $P_b = \frac{P_b^{(n)}}{\bar{t}_b^{*(n)}}$.
9: **end for**
10: Calculate $\epsilon = \max\{\frac{P_b}{P_{b,\max}}, \forall b \in \mathcal{B}; \sum_{b\in\mathcal{B}} \frac{P_b}{P_{tot}}\}$.
11: Update $\mathbf{P}^{(n+1)} = \frac{\mathbf{P}^{(n+1)}}{\epsilon}$, $n = n + 1$.
12: **until** $n > N_{\max}$ or $|\bar{t}_b^{*(n+1)} - \bar{t}_b^{*(n)}| < \xi_2$
13: $\bar{n} = \bar{n} + 1$.
14: Update timeslot assignment $\boldsymbol{\alpha}_b^{(\bar{n})}$.
15: **until** $\bar{n} > \bar{N}_{\max}$
16: Calculate p_{bkc} based on $\mathbf{P}^{(n)}$.

Output:
$\bar{t}_b^*$, p_{bkc}, $\boldsymbol{\alpha}_b$, $\mathbf{w}_{bc}$.

$$p_{bkc} \leq \hat{P}\alpha_{bkc}, \forall c \in \mathcal{C}, \forall k \in \mathcal{K}_b. \tag{18e}$$

The decoding order indicators ϕ_{bklc} are determined based on $\mathbf{P}$ and g_{bkc}. Thus variables ϕ_{bklc} are therefore fixed and constraints (7h) and (7i) are no longer needed in $\mathcal{P}_4(b)$. By expressing p_{bkc} by R_{bkc}, $\mathcal{P}_4(b)$ is reformulated as:

$$\mathcal{P}_5(b): \max_{R_{bkc},\alpha_{bkc},t_b} \quad t_b \tag{19a}$$

$$\text{s.t.} \quad (18\text{c}), (18\text{e}), (18\text{d}), \tag{19b}$$

$$\sum_{k=1}^{K_b} \left(\frac{1}{g_{bkc}} - \frac{1}{g_{b(k-1)c}}\right) e^{\sum_{j\geq k} \frac{R_{bjc}}{B_W}} - \frac{1}{g_{bK_bc}} \leq \frac{P_b}{\rho_{bc}}, \quad \forall c \in \mathcal{C}, \tag{19c}$$

$$t_b D_{bk} - R_{bk} \leq 0, \forall k \in \mathcal{K}_b, \tag{19d}$$

where the inequalities in (18b) are relaxed as the inequalities in (19c) to convert the constraints to exponential cones. Thus $\mathcal{P}_5(b)$ is identified as mixed-integer exponential conic programming (MIECP) [39], whose optimum can be solved by branch and bound or outer approximation approach.

Similar to $f_b(\mathbf{P}) = t_b^*$ in $\mathcal{P}_2(b)$, the optimal objective $\bar{t}_b^*$ in $\mathcal{P}_5(b)$ can be re-expressed by an inexplicit function of $\mathbf{P}$, say $\bar{f}_b(\mathbf{P})$. Based on Lemma 1 and Lemma 2, the objective function $f_b(\mathbf{P})$ in $\mathcal{P}_2(b)$ is a CUF. We then conclude that $\bar{f}_b(\mathbf{P})$ is also a CUF in Corollary 2.

Corollary 2: $\bar{f}_b(\mathbf{P})$ is a CUF.

TABLE II
SIMULATION PARAMETERS

Parameter	Value
Frequency	20 GHz (Ka band)
B_W	500 MHz
Satellite location	13° E [43]
Satellite height	35,786 km [43]
Beam radiation pattern	provided by ESA [43]
Receive antenna gain	42.1 dBi
Channel model	free-space propagation loss
σ^2	-126.47 dBW
B, C	4, 5
$P_{b,\max}$, P_{tot}	120 W, 400 W [20]
$\lvert\mathcal{U}_b\rvert$	70
K	2
D_{bk}	uniform distribution [44], traffic emulator in [3]
$N_{\max}$, $\bar{N}_{\max}$	15, 5

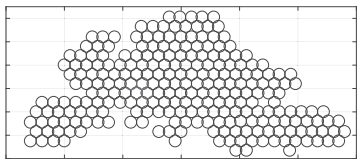

Fig. 2. Beam pattern covering Europe provided by European Space Agency [43]. The figure shows an instance of four beams (highlighted in red color) served by an MPA.

Proof: Please refer to Appendix D. ■

Owing to the linearity, the constraints in the formulation of $\mathcal{P}_3$ are MCs. With the properties of CUF and MC, the beam power allocation problem is an MCMU and can be tackled by the PF-based approach. By solving $\mathcal{P}_5$ in line 7, a new terminal-timeslot assignment is obtained (updated in line 14), and the optimal $\bar{t}_b^*(n)$ is achieved, which is used taso update beam power in line 8. The algorithm terminates when the number of iterations (line 2 to line 14) reaches $\bar{N}_{\max}$.

In Algorithm 2, there are at most $\bar{N}_{\max} N_{\max} B$ MIECPs to be solved. For each MIECP, the optimum can be obtained by branch and bound approach with exponential-time complexity [40]. For the worst-case scenario, the approach fathoms all the combinations of binary variables [41], resulting in solving $2^{K_b C}$ conic programmings. The complexity of solving a conic programming by interior-point method is $\mathcal{O}(-\nu \log \varepsilon_2)$ [42], where ν and ε_2 represent the self-concordant barrier parameter and precision. Thus the upper-bound complexity of Algorithm 2 is $\mathcal{O}(-\bar{N}_{\max} N_{\max} \sum_{b\in\mathcal{B}} 2^{K_b C} \nu \log \varepsilon_2)$. Note that the global optimum of $\mathcal{P}_0$ is absent. Algorithm 2 with exponential complexity aims at providing benchmarks and upper bounds for low-complexity algorithms.

VI. PERFORMANCE EVALUATION

A. Parameter Settings

We evaluate the performance of the proposed resource allocation approaches in a NOMA-enabled multi-beam satellite system. The key parameters are summarized in Table II. The parameters related to the satellite and beam radiation patterns are provided by European Space Agency (ESA) [43]. The power parameters follow the typical values in [20]. Fig. 2 illustrates the beam pattern we consider. In the system, a small cluster

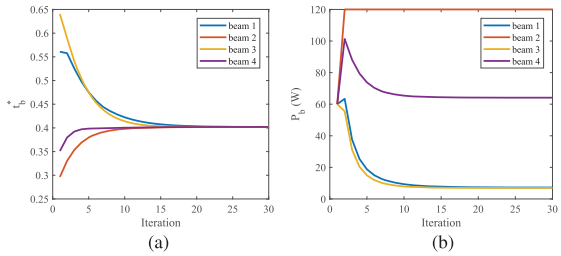

Fig. 3. Evolutions of t_b^* and P_b over iterations in JOPD.

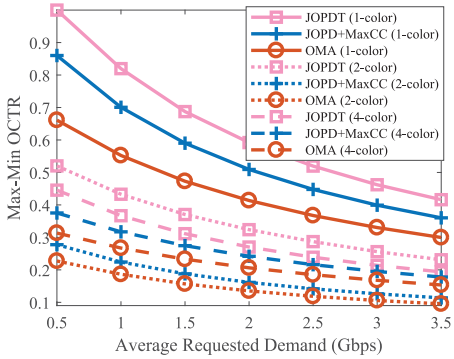

Fig. 4. Max-min OCTR with respect to traffic demand among JOPDT, JOPD+MaxCC, and OMA.

of co-channel beams ($B = 4$) is served by an MPA. Note that the variation of transmit antenna gain is related to the off-axis angle between the beam center and the terminal. In NOMA, since the complexity of multi-user detection increases with the number of signals to be detected by the receiver [9], $\bar{K} = 2$ is set in the simulation unless otherwise stated. The results are averaged over 1000 instances. For each instance, one terminal is randomly selected from $\mathcal{U}_b$ and the other is paired via MaxCC for each timeslot. Two NOMA-based schemes, i.e., JOPD+MaxCC with lower complexity and JOPDT with higher complexity, are compared to OMA and other benchmarks.

B. Numerical Results

1) Convergence of JOPD: We first verify the convergence performance of JOPD. Fig. 3 shows the evolutions of t_b^* and P_b over iterations. From the figures, we observe that beam power is adjusted based on the values of t_b^*. The power of the beams with smaller t_b^* increases while the power of the other beams decreases in each iteration. As it is proven in Theorem 1, JOPD converges, e.g., in Fig. 3(a) within around 15 iterations. Besides, the results verify the conclusion of Lemma 2, that is, the convergence of a CUF is not affected by the variation of decoding orders.

2) Comparison of Max-Min OCTR Between NOMA and OMA: Next, we compare the max-min OCTR performance among JOPDT, JOPD+MaxCC, and OMA in Fig. 4 to verify the superiority of the proposed NOMA-based schemes. Different frequency-reuse patterns, i.e., 1-color, 2-color, and 4-color frequency-reuse patterns, are implemented. In 1-color frequency-reuse pattern, the entire bandwidth is shared by all the spot beams. 2-color (or 4-color) pattern refers to the scenarios that the bandwidth is equally divided into 2 (or 4) portions, each of which is occupied by one of the 2 (or 4) adjacent beams. In

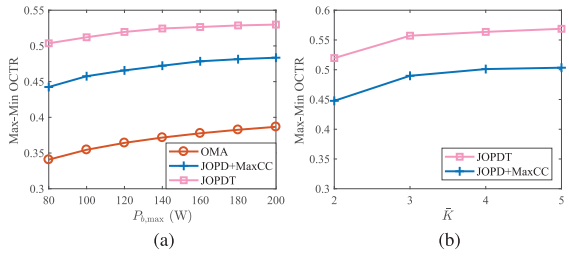

Fig. 5. Max-min OCTR with respect to: (a), $P_{b,\max}$; (b), $\bar{K}$, among JOPDT, JOPD+MaxCC, and OMA.

OMA, the available frequency band is halved. Each half of the band is occupied by one terminal at each timeslot. Note that terminals are paired and scheduled to each timeslot by MaxCC in OMA.

In average, JOPD with MaxCC outperforms OMA with MaxCC in max-min OCTR by 24.0%, 20.0%, and 17.5% under 1-color, 2-color, and 4-color pattern, respectively. Particularly, with the implementation of 1-color pattern, the max-min OCTR in JOPD is 30.1% higher than that in OMA when the average requested demand is 0.5 Gbps. JOPD coordinated with precoding and MaxCC benefits from both reduced inter-beam and intra-beam interference compared to OMA. Remark that in 2-color pattern, both JOPD+MaxCC and OMA are worse than other frequency-reuse patterns. The reason is that compared to 2-color pattern, precoding is more effective in 1-color to mitigate strong inter-beam interference to a large extent, whereas 4-color pattern inherently receives much less inter-beam interference than that of 2-color pattern. Besides, the OCTR performance of JOPD+MaxCC is compared with JOPDT. By taking into account optimizing the terminal-timeslot assignment, JOPDT is able to improve the max-min fairness by approximately 16.2%, 98.2%, and 12.7% under 1-color, 2-color, and 4-color reuse patterns, respectively. The results validate the improvement of JOPDT over JOPD by iteratively updating the terminal-timeslot assignment.

In Fig. 5(a), we present the OCTR performance among JOPD+MaxCC, JOPDT, and OMA, with respect to $P_{b,\max}$. By using higher beam power $P_{b,\max}$, the max-min-OCTR value in all the three algorithms can be improved, but not significant. This might suggest that, to improve the worst-OCTR terminal's performance in practice, developing advanced user-scheduling and power-allocation schemes would be the key rather than simply increasing beam power.

In Fig. 5(b), we show the OCTR performance with various $\bar{K}$ for the proposed two algorithms. The max-min OCTR in two NOMA schemes increases effectively when $\bar{K}$ grows from 2 to 3. The growth becomes slow when 4 to 5 terminals are multiplexed on each slot. As we mentioned before, higher $\bar{K}$ might not necessarily bring significant improvement but imposes more complexity to multi-user detection and SIC at the receiver side. Thus, in the simulation, we set $\bar{K} = 2$ for the trade-off between performance gain and complexity.

3) Comparison of Max-Min OCTR Among Different Terminal-Timeslot Allocations: Different strategies of terminal-timeslot scheduling are compared in Fig. 6 in order to illustrate the advantages of MaxCC with NOMA in improving OCTR

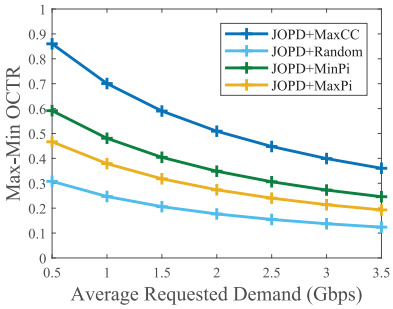

Fig. 6. Max-min OCTR with respect to traffic demand among different terminal-timeslot assignment approaches.

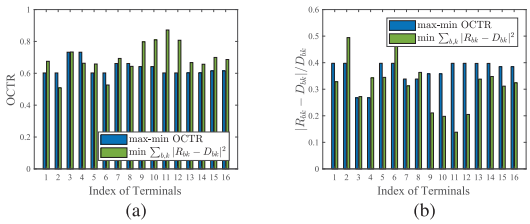

Fig. 7. An illustration of the distribution of (a) OCTR; (b) Ratio $|R_{bk} - D_{bk}|/D_{bk}$ among terminals achieved by max-min OCTR and min $\sum_{b,k} |R_{bk} - D_{bk}|^2$.

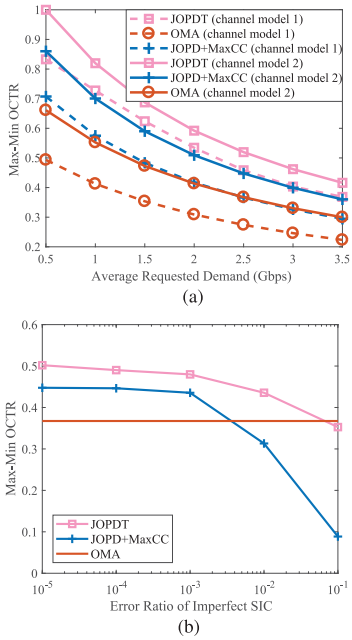

Fig. 8. Max-min OCTR comparison: (a) by adopting two channel models: 1, atmospheric-fading model based on ITU-R P.1853-2 [46], 2, free-space model; (b) considering error ratio of imperfect SIC.

performance. The basis of MaxCC is to allocate each timeslot to terminals with highest-correlation channels without considering the gap of $\|\mathbf{h}_{bk}\|$. The benchmarks are listed as follows:

- MaxPi [8]: Allocate each timeslot to terminals with highly correlated channels and the largest gap of $\|\mathbf{h}_{bk}\|$,
- MinPi [8]: Allocate each timeslot to terminals with highly correlated channels and the smallest gap of $\|\mathbf{h}_{bk}\|$,
- Random: Allocate each timeslot to terminals randomly.

Note that in MaxPi and MinPi, terminals with the largest and smallest gain difference, respectively, are selected from those with correlation factor $\theta > 0.9$.

From Fig. 6, JOPD+MaxCC brings the largest gain compared to other benchmarks. In MaxCC, the terminals with the highest channel correlation are selected. Hence MaxCC can effectively reduce the inter-beam interference and exploit the synergy of NOMA with precoding. Besides, the OCTR performance is sensitive to inter-beam interference. The non-highest correlated channels in MinPi and MaxPi introduce a considerable amount of inter-beam interference and thus degrade the performance to a certain extent.

4) Metrics Comparison Between "max-Min OCTR" and "min $\sum_{b,k} |R_{bk} - D_{bk}|^2$*":* Fig. 7(a) presents the distribution of OCTRs among terminals achieved by JOPD+MaxCC, compared with NOMA to minimize $\sum_{b,k} |R_{bk} - D_{bk}|^2$. Previous works, e.g., [20], [45], focus on reducing the sum of the gap between offered capacity and requested traffic demand, i.e., "min $\sum_{b,k} |R_{bk} - D_{bk}|^2$". The approach proposed in [28] is adopted to solve the problem with the objective of "min $\sum_{b,k} |R_{bk} - D_{bk}|^2$". We can observe that the max-min operator compromises the performance of high-capacity terminals, e.g., terminals 9 to 12, to compensate terminals with low OCTRs, e.g., terminals 2 and 6. The average OCTR in "max-min OCTR" is lower than that in "min $\sum_{b,k} |R_{bk} - D_{bk}|^2$" by 8.82%, but the minimum OCTR increases by 18.4% in "max-min OCTR".

We evaluate the performance of "max-min OCTR" and "min $\sum_{b,k} |R_{bk} - D_{bk}|^2$" by another metric, $\frac{|R_{bk}-D_{bk}|}{D_{bk}}$, in Fig. 7(b). The performance in "min $\sum_{b,k} |R_{bk} - D_{bk}|^2$" achieves 14.78% higher average performance but loses of 19.54% in the worst $\frac{|R_{bk}-D_{bk}|}{D_{bk}}$ than "max-min OCTR". In addition, by adopting the Jain fairness index [4], i.e., $(\sum_{b,k} \frac{R_{bk}}{D_{bk}})^2/((\sum_b K_b)\sum_{b,k}(\frac{R_{bk}}{D_{bk}})^2)$, the performance in both functions "max-min OCTR" and "min $\sum_{b,k} |R_{bk} - D_{bk}|^2$" leads to satisfactory fairness values 0.99 and 0.98, respectively.

5) Evaluation in the Scenarios With Pracitcal Factors: In Fig. 8, we evaluate the max-min OCTR among the three algorithms when practical factors are considered. The performance achieved by the three schemes over the channels with free-space propagation loss and with atmospheric fading is compared in Fig. 8(a). The channel model with atmospheric fading (consisting of long-term effects and rain effects) is emulated based on Recommendation ITU-R P.1853-2 [46]. From the results, firstly, we observe that the performance improvement of the proposed two NOMA schemes, i.e., JOPDT and JOPD+MaxCC, over OMA is consistent in both channel models. Secondly, the benefits of adopting NOMA in the atmospheric-fading model over OMA are even more significant than that in the free-space cases.

In Fig. 8(b), we investigate the OCTR performance under imperfect-SIC conditions. We adopt an approach proposed in [29] which uses an error ratio to represent the residual intra-beam interference due to error propagation of imperfect SIC. With a lower error ratio, e.g., from 10^{-5} to 10^{-3}, the performance of both NOMA schemes slightly decreases, but keeps considerable performance gain over OMA. However, as the error ratio

increases, this performance gain can be diminished because a non-negligible residual interference has to be taken into account in NOMA but this type of interference does not present in OMA. The NOMA performance can be lower than that of OMA when error ratios are very high, e.g., 10^{-2} and 10^{-1}. This suggests that to maintain the advantages of NOMA in practice, the error ratio of SIC has to be confined at low levels, otherwise OMA might be a more favorable option. In addition, we observe that JOPDT is more robust than JOPD+MaxCC in against imperfect SIC. This is because that when the error ratio and the resulting interference become non-negligible, JOPDT is able to properly update the terminal groups iteratively whereas JOPD+MaxCC has to keep the fixed terminal-timeslot assignment.

VII. Conclusion

In this paper, we have introduced NOMA into multi-beam satellite systems to enable aggressive frequency reuse and enhance spectral efficiency. A max-min problem of jointly optimizing power, decoding orders, and terminal-timeslot assignment has been formulated to improve the worst OCTR among terminals. We have proposed a PF-based algorithmic framework JOPD to jointly allocate power and decide decoding orders by fixing terminal-timeslot assignment with the guarantee of fast convergence. Based on the framework of JOPD, a heuristic approach JOPDT has been developed to iteratively update the terminal-timeslot assignment and improve the overall OCTR performance. The superiority of the proposed algorithms in max-min fairness over OMA has been demonstrated.

Appendix A
Proof of Proposition 1

Proof: We can obtain the optimum of the relaxed problem based on KKT conditions. The corresponding Lagrangian dual function is:

$$\mathcal{L}(R_{bkc}, t_b; \lambda_c, \mu_k) = -t_b + \sum_{c\in\mathcal{C}} \lambda_c \left(\sum_{k=1}^{K_b} \left(\frac{1}{g_{bkc}} - \frac{1}{g_{b(k-1)c}} \right) e^{\sum_{j\geq k} \frac{R_{bjc}}{B_W}} - \frac{1}{g_{bK_bc}} - \frac{P_b}{\rho_{bc}} \right) + \sum_{k=1}^{K_b} \mu_k (tD_{bk} - R_{bk}), \tag{20}$$

where $\lambda_c \geq 0$ and $\mu_k \geq 0$ are Lagrangian multipliers for constraints (13) and (12b), respectively. The KKT conditions can be derived as

$$\frac{\partial \mathcal{L}}{\partial R_{bkc}} = \lambda_c \sum_{n=1}^{k} \left(\frac{1}{g_{bnc}} - \frac{1}{g_{b(n-1)c}} \right) e^{\sum_{j\geq n} \frac{R_{bjc}}{B_W}} - \mu_k = 0, \quad \forall c \in \mathcal{C}, k \in \mathcal{K}_b, \tag{21a}$$

$$\frac{\partial \mathcal{L}}{\partial t} = -1 + \sum_{k=1}^{K_b} \mu_k D_{bk} = 0, \tag{21b}$$

$$\lambda_c \left(\sum_{k=1}^{K_b} \left(\frac{1}{g_{bkc}} - \frac{1}{g_{b(k-1)c}} \right) e^{\sum_{j\geq k} \frac{R_{bjc}}{B_W}} - \frac{1}{g_{bK_bc}} - \frac{P_b}{\rho_{bc}} \right) = 0, \quad \forall c \in \mathcal{C}, \tag{21c}$$

$$\mu_k (t_b D_{bk} - R_{bk}) = 0, \forall k \in \mathcal{K}_b. \tag{21d}$$

At the optimum of $\mathcal{P}_1(b)$, at least one constraint in (12b), say the k^*-th constraint/terminal, will be active, i.e., the equality holds, whereas the others keep inequalities [39]. The optimal value t_b^* is then achieved at the equality $t_b^* D_{bk^*} - R_{bk^*} = 0$ [35], [39]. In (21d), for the inequality terms $t_b^* D_{bk} - R_{bk} < 0$, the corresponding μ_k must be zero, while for the equality term $t_b^* D_{bk^*} - R_{bk^*} = 0$, $\mu_{k^*} > 0$ instead of zero since (21b) cannot hold for all-zero μ_k. Hence, the optimal t_b^* is associated with positive μ_k^*. The positive μ_k^* in (21a) results in positive λ_c which leads to $\sum_{k=1}^{K_b} (\frac{1}{g_{bkc}} - \frac{1}{g_{b(k-1)c}}) e^{\sum_{j\geq k} \frac{R_{bjc}}{B_W}} - \frac{1}{g_{bK_bc}} - \frac{P_b}{\rho_{bc}} = 0$ in (21c). Thus the conclusion. ■

Appendix B
Proof of Lemma 1

Proof: Given any $\mathbf{P}$ and the corresponding decoding order, according to Definition 1, we check the three conditions for $f_b(\mathbf{P}), \forall b \in \mathcal{B}$.

Positivity: Rewrite (16) equivalently as:

$$\sum_{k=1}^{K_b-1} \frac{1}{g_{bkc^*}} e^{\sum_{j>k} \frac{t_b^* D_{bj}}{B_W}} (e^{\frac{t_b^* D_{bk}}{B_W}} - 1) + \frac{1}{g_{bK_bc^*}} (e^{\frac{t_b^* D_{bK_b}}{B_W}} - 1) = \frac{P_b}{\rho_{bc^*}}. \tag{22}$$

The right-hand side is positive, then the term $e^{\frac{t_b^* D_{bk}}{B_W}} - 1$ in the left-hand side has to keep positive. Hence t_b^* is positive.

Competitiveness: By deriving the partial derivatives of $f_b(\mathbf{P})$, i.e., $\frac{\partial f_b}{\partial P_b}$ and $\frac{\partial f_b}{\partial P_{b'}}$ in (23) and (24), shown at bottom of this page, respectively, we observe $\frac{\partial f_b}{\partial P_b} > 0$ and $\frac{\partial f_b}{\partial P_{b'}} < 0$, which means that $f_b(\mathbf{P})$ monotonically increases with beam b's power P_b but decreases with any other beam's power $P_{b'}$.

$$\frac{\partial f_b}{\partial P_b} = \frac{1}{\sum_{k=1}^{K_b} \left(\frac{1}{g_{bkc^*}} - \frac{1}{g_{b(k-1)c^*}} \right) e^{\sum_{j\geq k} \frac{t_b^* D_{bj}}{B_W}} \sum_{j\geq k} \frac{D_{bj}}{B_W}} \tag{23}$$

$$\frac{\partial f_b}{\partial P_{b'}} = -\frac{\sum_{k=1}^{K_b-1} \frac{|\mathbf{h}_{bk}^H \mathbf{w}_{b'c^*}|^2}{|\mathbf{h}_{bk}^H \mathbf{w}_{bc^*}|^2 \rho_{bc^*}} e^{\sum_{j>k} \frac{t_b^* D_{bj}}{B_W}} (e^{\frac{t_b^* D_{bk}}{B_W}} - 1) + \frac{|\mathbf{h}_{bK_b}^H \mathbf{w}_{b'c^*}|^2}{|\mathbf{h}_{bK_b}^H \mathbf{w}_{bc^*}|^2 \rho_{bc^*}} (e^{\frac{t_b^* D_{bK_b}}{B_W}} - 1)}{\sum_{k=1}^{K_b} \left(\frac{1}{g_{bkc^*}} - \frac{1}{g_{b(k-1)c^*}} \right) e^{\sum_{j\geq k} \frac{t_b^* D_{bj}}{B_W}} \sum_{j\geq k} \frac{D_{bj}}{B_W}} \tag{24}$$

Directional Monotonicity: Let $\zeta > 1$. We assume $f_b(\zeta\mathbf{P}) = \tau_1$ and $f_b(\mathbf{P}) = \tau_2$. From equation (16), τ_1 can be derived by the following equation:

$$\sum_{k=1}^{K_b-1} \frac{1}{\hat{f}_{bkc^*}(\zeta\bar{\mathbf{P}}_b)} e^{\sum_{j>k} \frac{\tau_1 D_{bj}}{B_W}} (e^{\frac{\tau_1 D_{bk}}{B_W}} - 1) + \frac{1}{\hat{f}_{bK_bc^*}(\zeta\bar{\mathbf{P}}_b)} (e^{\frac{\tau_1 D_{bK_b}}{B_W}} - 1) - \frac{\zeta P_b}{\rho_{bc^*}} = 0. \quad (25)$$

By substituting $f_b(\mathbf{P}) = \tau_2$ into (16), both sides of the equation multiply ζ, i.e.,

$$\sum_{k=1}^{K_b-1} \frac{\zeta}{\hat{f}_{bkc^*}(\bar{\mathbf{P}}_b)} e^{\sum_{j>k} \frac{\tau_2 D_{bj}}{B_W}} (e^{\frac{\tau_2 D_{bk}}{B_W}} - 1) + \frac{\zeta}{\hat{f}_{bK_bc^*}(\bar{\mathbf{P}}_b)} (e^{\frac{\tau_2 D_{bK_b}}{B_W}} - 1) - \frac{\zeta P_b}{\rho_{bc^*}} = 0. \quad (26)$$

Based on the equation in (4), we can derive $\frac{1}{\hat{f}_{bkc^*}(\zeta\bar{\mathbf{P}})} < \frac{\zeta}{\hat{f}_{bkc^*}(\bar{\mathbf{P}})}$ by:

$$\frac{1}{\hat{f}_{bkc^*}(\zeta\bar{\mathbf{P}})} = \frac{\sum_{b'\neq b} |\mathbf{h}_{bk}^H \mathbf{w}_{b'c^*}|^2 \zeta \frac{P_{b'}}{\rho_{b'c^*}} + \sigma^2}{|\mathbf{h}_{bk}^H \mathbf{w}_{bc^*}|^2} < \zeta \frac{\sum_{b'\neq b} |\mathbf{h}_{bk}^H \mathbf{w}_{b'c^*}|^2 \frac{P_{b'}}{\rho_{b'c^*}} + \sigma^2}{|\mathbf{h}_{bk}^H \mathbf{w}_{bc^*}|^2} = \frac{\zeta}{\hat{f}_{bkc^*}(\bar{\mathbf{P}}_b)}. \quad (27)$$

Based on (27), the terms $\frac{1}{\hat{f}_{bkc^*}(\zeta\bar{\mathbf{P}})}$ and $\frac{1}{\hat{f}_{bK_bc^*}(\zeta\bar{\mathbf{P}})}$ in (25) are smaller than $\frac{\zeta}{\hat{f}_{bkc^*}(\bar{\mathbf{P}}_b)}$ and $\frac{\zeta}{\hat{f}_{bK_bc^*}(\bar{\mathbf{P}}_b)}$ in (26), respectively. Hence, the equalities in (25) and (26) cannot hold under both cases $\tau_1 = \tau_2$ and $\tau_1 < \tau_2$. Thus $\tau_1 > \tau_2$ and $f_b(\zeta\mathbf{P}) > f_b(\mathbf{P})$.■

APPENDIX C
PROOF OF LEMMA 2

Proof: Positivity: The positivity of $f_b(\mathbf{P})$ holds whether the decoding order changes or not according to (22).

Competitiveness: The decoding order in beam b depends on $\bar{\mathbf{P}}_b$. Given any two terminals k and k' in beam b, suppose that in beam b', there exist $P_{b'}$ and δ such that $P_{b'}$ leads to $g_{bkc} = g_{bk'c}$; setting $P_{b'} - \delta$ results in terminal k decoding k' ($g_{bkc} > g_{bk'c}$); and $P_{b'} + \delta$ changes the decoding order to k' decoding k ($g_{bkc} < g_{bk'c}$). $f_b(\mathbf{P})$ is competitive when the decoding order stays unchanged. When $g_{bkc} = g_{bk'c}$, $f_b(\mathbf{P})$ remains the same under both decoding orders. Thus $f_b(\mathbf{P})$ is continuous, indicating that $f_b(\mathbf{P})$ monotonically decreases in $P_{b'}$ even if the decoding order changes. The competitiveness is concluded.

Directional monotonicity: Assume that the decoding order changes from k decoding k' to k' decoding k as the beam power increases from $\mathbf{P}$ to $\zeta\mathbf{P}$, where $\zeta > 1$. There exists ζ_0, where $1 < \zeta_0 < \zeta$, such that $\zeta_0\mathbf{P}$ corresponds to $g_{bkc} = g_{bk'c}$. As proven in Lemma 1, $f_b(\mathbf{P}) < f_b(\zeta_0\mathbf{P})$ and $f_b(\zeta_0\mathbf{P}) < f_b(\zeta\mathbf{P})$. Thus $f_b(\mathbf{P}) < f_b(\zeta\mathbf{P})$. ■

APPENDIX D
PROOF OF THEOREM 1

Proof: At the optimum, $f_b(\mathbf{P}^*) = t^*$, $\forall b \in \mathcal{B}$, where $\mathbf{P}^* = [P_1^*, \ldots, P_b^*, \ldots, P_B^*]$ and t^* are the optimal beam power and the optimal OCTR value, respectively. Define function $\eta_b(\mathbf{P}) = \frac{P_b}{f_b(\mathbf{P})}$, $\forall b \in \mathcal{B}$. At the convergence, $\frac{P_b^*}{t^*} = \frac{P_b^*}{f_b(\mathbf{P}^*)}$, $\forall b \in \mathcal{B}$.

The algorithm converges geometrically fast to t^* with any initial $\mathbf{P}$ if $\eta_b(\mathbf{P})$ satisfies the following conditions [47]:

- There exist $\underline{\tau}$ and $\overline{\tau}$, where $0 < \underline{\tau} \leq \overline{\tau}$, such that $\underline{\tau} \leq \eta_b(\mathbf{P}) \leq \overline{\tau}$, $\forall b \in \mathcal{B}$.
- For any beam power $\mathbf{P}_1 \succ \mathbf{0}$ and $\mathbf{P}_2 \succ \mathbf{0}$, and $0 < \zeta \leq 1$, if $\zeta\mathbf{P}_1 \preceq \mathbf{P}_2$, then $\zeta\eta_b(\mathbf{P}_1) \leq \eta_b(\mathbf{P}_2)$, $\forall b \in \mathcal{B}$. For $0 < \zeta < 1$, if $\zeta\mathbf{P}_1 \prec \mathbf{P}_2$, then $\zeta\eta_b(\mathbf{P}_1) < \eta_b(\mathbf{P}_2)$, $\forall b \in \mathcal{B}$.

For the first condition, $\eta_b(\mathbf{P})$ stays between $\underline{\tau}$ and $\overline{\tau}$, which means the function could not be zero or infinite with any $\mathbf{P}$. Due to the positivity of $f_b(\mathbf{P})$, $\eta_b(\mathbf{P}) = \frac{P_b}{f_b(\mathbf{P})} > 0$, i.e., $\eta_b(\mathbf{P}) \geq \underline{\tau} > 0$. Since $\mathbf{P}$ is bounded by $P_{b,\max}$, $\eta_b(\mathbf{P})$ is finite. Thus the function is upper bounded, i.e., $\eta_b(\mathbf{P}) \leq \overline{\tau}$.

For the second condition, we prove $\zeta\eta_b(\mathbf{P}_1) \leq \eta_b(\mathbf{P}_2)$ via showing the inequality below.

$$\zeta\eta_b(\mathbf{P}_1) \leq \eta_b(\zeta\mathbf{P}_1) \leq \eta_b(\mathbf{P}_2). \quad (28)$$

The first inequality $\zeta\eta_b(\mathbf{P}_1) \leq \eta_b(\zeta\mathbf{P}_1)$ reads,

$$\frac{\zeta P_b}{f_b(\mathbf{P}_1)} \leq \frac{\zeta P_b}{f_b(\zeta\mathbf{P}_1)}. \quad (29)$$

Let $\zeta\mathbf{P}_1 = \mathbf{P}$, then $\mathbf{P}_1 = \frac{1}{\zeta}\mathbf{P}$, where $\frac{1}{\zeta} \geq 1$. According to Lemma 1 and Lemma 2, $f_b(\mathbf{P})$ satisfies directional monotonicity, thus $f_b(\frac{1}{\zeta}\mathbf{P}) \geq f_b(\mathbf{P})$ and $\zeta\eta_b(\mathbf{P}_1) \leq \eta_b(\zeta\mathbf{P}_1)$ holds. For the second inequality in (28), $\eta_b(\zeta\mathbf{P}_1) \leq \eta_b(\mathbf{P}_2)$. Based on $\frac{\partial f_b}{\partial P_b} > 0$ and $\frac{\partial f_b}{\partial P_{b'}} < 0$ in (23) and (24), we can derive the partial derivatives of $\eta_b(\mathbf{P})$ as $\frac{\partial \eta_b}{\partial P_b} = \frac{f_b(\mathbf{P}) - P_b \frac{\partial f_b}{\partial P_b}}{f_b^2(\mathbf{P})}$, and $\frac{\partial \eta_b}{\partial P_{b'}} = -\frac{P_b \frac{\partial f_b}{\partial P_{b'}}}{f_b^2(\mathbf{P})}$, where $\frac{\partial \eta_b}{\partial P_{b'}}$ is positive. We derive $\frac{\partial^2 f_b}{\partial P_b^2} < 0$ based on (23), which indicates the concavity of $f_b(\mathbf{P})$ on P_b [39]. Let $\mathbf{P}_0 = [P_1, \ldots, 0, \ldots, P_B]$. According to the first-order condition of concavity [39] and $f_b(\mathbf{P}_0) = 0$, $f_b(\mathbf{P}) - f_b(\mathbf{P}_0) > (P_b - 0)\frac{\partial f_b}{\partial P_b}$, and thus $\frac{\partial \eta_b}{\partial P_b} = \frac{f_b(\mathbf{P}) - P_b \frac{\partial f_b}{\partial P_b}}{f_b^2(\mathbf{P})} > 0$. The monotonicity of $\eta_b(\mathbf{P})$ is concluded, i.e., $\eta_b(\mathbf{P})$ is an increasing function of $\mathbf{P}$. Hence $\eta_b(\zeta\mathbf{P}_1) \leq \eta_b(\mathbf{P}_2)$ holds in (28), and thus $\zeta\eta_b(\mathbf{P}_1) \leq \eta_b(\mathbf{P}_2)$. The result that $\zeta\eta_b(\mathbf{P}_1) < \eta_b(\mathbf{P}_2)$ if $\zeta_0\mathbf{P}_1 \prec \mathbf{P}_2$ follows analogously. ■

APPENDIX E
PROOF OF COROLLARY 2

Proof: The properties of positivity and competitiveness follow analogously from Lemma 1 and Lemma 2. Regarding the directional monotonicity, given $\zeta\mathbf{P}$ and $\mathbf{P}$ to $\mathcal{P}_5(b)$, we can obtain the optimal terminal-timeslot allocation $\boldsymbol{\alpha}_1^*$ and $\boldsymbol{\alpha}_2^*$, respectively, where $\boldsymbol{\alpha}_1^*$ and $\boldsymbol{\alpha}_2^*$ collect all α-variables in beam b. Note that the difference between $\mathcal{P}_5(b)$ and $\mathcal{P}_2(b)$ is that α_{bkc} is treated as fixed parameters in $\mathcal{P}_2(b)$, whereas α_{bkc} is to be optimized in $\mathcal{P}_5(b)$ as variables. Thus, under the same $\boldsymbol{\alpha}_2^*$ in $\mathcal{P}_2(b)$, $f_b(\zeta\mathbf{P}) > f_b(\mathbf{P})$ can hold for $\zeta > 1$ according to Lemma 1 and Lemma 2. Since $\boldsymbol{\alpha}_2^*$ is the optimal outcome of using $\mathbf{P}$ in $\mathcal{P}_5(b)$, then $\bar{f}_b(\mathbf{P}) = f_b(\mathbf{P})$. Compared with $f_b(\zeta\mathbf{P})$ and $\bar{f}_b(\zeta\mathbf{P})$, $f_b(\zeta\mathbf{P})$ with a suboptimal $\boldsymbol{\alpha}_2^*$ is no higher than $\bar{f}_b(\zeta\mathbf{P})$ with its optimal $\boldsymbol{\alpha}_1^*$, thus $\bar{f}_b(\zeta\mathbf{P}) > f_b(\zeta\mathbf{P})$, and $\bar{f}_b(\zeta\mathbf{P}) > \bar{f}_b(\mathbf{P})$, then the conclusion. ■

REFERENCES

[1] A. I. Pérez-Neira, M. Á. Vázquez, M. R. B. Shankar, S. Maleki, and S. Chatzinotas, "Signal processing for high-throughput satellites: Challenges in new interference-limited scenarios," *IEEE Signal Process. Mag.*, vol. 36, no. 4, pp. 112–131, Jul. 2019.

[2] O. Kodheli *et al.*, "Satellite communications in the new space era: A survey and future challenges," *IEEE Commun. Surveys Tut.*, p. 1, Oct. 2020.

[3] (SIGCOM) (SnT), "Satellite Traffic Emulator," University of Luxembourg, Luxembourg. [Online]. Available: https://wwwfr.uni.lu/snt/research/sigcom/sw_simulators/satellite_traffic_emulator

[4] G. Cocco, T. De Cola, M. Angelone, Z. Katona, and S. Erl, "Radio resource management optimization of flexible satellite payloads for DVB-S2 systems," *IEEE Trans. Broadcast.*, vol. 64, no. 2, pp. 266–280, Jun. 2018.

[5] L. Lei *et al.*, "Learning-assisted optimization for energy-efficient scheduling in deadline-aware NOMA systems," *IEEE Trans. Green Commun. Netw.*, vol. 3, no. 3, pp. 615–627, Sep. 2019.

[6] S. R. Islam, N. Avazov, O. A. Dobre, and K.-S. Kwak, "Power-domain non-orthogonal multiple access (NOMA) in 5G systems: Potentials and challenges," *IEEE Commun. Surveys Tut.*, vol. 19, no. 2, pp. 721–742, Oct. 2016.

[7] E. Okamoto and H. Tsuji, "Application of non-orthogonal multiple access scheme for satellite downlink in satellite/terrestrial integrated mobile communication system with dual satellites," *IEICE Trans. Commun.*, vol. 99, no. 10, pp. 2146–2155, 2016.

[8] M. Caus, M. Á. Vázquez, and A. I. "Pérez-neira, NOMA and interference limited satellite scenarios," in *Proc. 50th Asilomar Conf. Signals, Syst. Comput.*, 2016, pp. 497–501.

[9] A. I. Pérez-Neira, M. Caus, and M. Á. Vázquez, "Non-orthogonal transmission techniques for multibeam satellite systems," *IEEE Commun. Mag.*, vol. 57, no. 12, pp. 58–63, Dec. 2019.

[10] X. Yan *et al.*, "The application of power-domain non-orthogonal multiple access in satellite communication networks," *IEEE Access*, vol. 7, pp. 63 531–63 539, 2019.

[11] X. Yan, H. Xiao, C.-X. Wang, K. An, A. T. Chronopoulos, and G. Zheng, "Performance analysis of NOMA-based land mobile satellite networks," *IEEE Access*, vol. 6, pp. 31327–31339, 2018.

[12] X. Yue *et al.*, "Outage behaviors of NOMA-based satellite network over shadowed-rician fading channels," *IEEE Trans. Veh. Technol.*, vol. 69, no. 6, pp. 6818–6821, Jun. 2020.

[13] X. Zhu, C. Jiang, L. Kuang, N. Ge, and J. Lu, "Non-orthogonal multiple access based integrated terrestrial-satellite networks," *IEEE J. Sel. Areas Commun.*, vol. 35, no. 10, pp. 2253–2267, Oct. 2017.

[14] Z. Lin, M. Lin, J.-B. Wang, T. de Cola, and J. Wang, "Joint beamforming and power allocation for satellite-terrestrial integrated networks with non-orthogonal multiple access," *IEEE J. Sel. Topics Signal Process.*, vol. 13, no. 3, pp. 657–670, Jun. 2019.

[15] X. Liu, X. Zhai, W. Lu, and C. Wu, "QoS-guarantee resource allocation for multibeam satellite industrial Internet of Things with NOMA," *IEEE Trans. Ind. Informat.*, vol. 17, no. 3, pp. 2052–2061, Mar. 2021.

[16] L. You, D. Yuan, L. Lei, S. Sun, S. Chatzinotas, and B. Ottersten, "Resource optimization with load coupling in multi-cell NOMA," *IEEE Trans. Wireless Commun.*, vol. 17, no. 7, pp. 4735–4749, Jul. 2018.

[17] Z. Liu, L. Lei, N. Zhang, G. Kang, and S. Chatzinotas, "Joint beamforming and power optimization with iterative user clustering for MISO-NOMA systems," *IEEE Access*, vol. 5, pp. 6872–6884, 2017.

[18] S. Chinnadurai, P. Selvaprabhu, and M. H. Lee, "A novel joint user pairing and dynamic power allocation scheme in MIMO-NOMA system," in *Proc. Int. Conf. Inf. Commun. Technol. Convergence*, 2017, pp. 951–953.

[19] S. Ali, E. Hossain, and D. I. Kim, "Non-orthogonal multiple access (NOMA) for downlink multiuser MIMO systems: User clustering, beamforming, and power allocation," *IEEE Access*, vol. 5, pp. 565–577, 2016.

[20] A. I. Aravanis, M. R. B. Shankar, P.-D. Arapoglou, G. Danoy, P. G. Cottis, and B. Ottersten, "Power allocation in multibeam satellite systems: A two-stage multi-objective optimization," *IEEE Trans. Wireless Commun.*, vol. 14, no. 6, pp. 3171–3182, Jun. 2015.

[21] A. Wang, L. Lei, E. Lagunas, A. I. Pérez-Neira, S. Chatzinotas, and B. Ottersten, "On fairness optimization for NOMA-enabled multi-beam satellite systems," in *Proc. IEEE 30th Annu. Int. Symp. Pers., Indoor Mobile Radio Commun.*, 2019, pp. 1–6.

[22] D. Christopoulos, S. Chatzinotas, and B. Ottersten, "Multicast multigroup precoding and user scheduling for frame-based satellite communications," *IEEE Trans. Wireless Commun.*, vol. 14, no. 9, pp. 4695–4707, Sep. 2015.

[23] M. G. Kibria, E. Lagunas, N. Maturo, D. Spano, H. Al-Hraishawi, and S. Chatzinotas, "Carrier aggregation in multi-beam high throughput satellite systems," in *Proc. IEEE Glob. Commun. Conf.*, 2019, pp. 1–6.

[24] C. Mosquera, R. López-Valcarce, T. Ramírez, and V. Joroughi, "Distributed precoding systems in multi-gateway multibeam satellites: Regularization and coarse beamforming," *IEEE Trans. Wirel. Commun.*, vol. 17, no. 10, pp. 6389–6403, Oct. 2018.

[25] P. Angeletti and R. De Gaudenzi, "A pragmatic approach to massive MIMO for broadband communication satellites," *IEEE Access*, vol. 8, pp. 132 212–132 236, 2020.

[26] N. Fatema, G. Hua, Y. Xiang, D. Peng, and I. Natgunanathan, "Massive MIMO linear precoding: A. survey," *IEEE Syst. J.*, vol. 12, no. 4, pp. 3920–3931, Dec. 2018.

[27] ETSI EN 301 307–2, "Digital Video Broadcasting (DVB); Second Generation Framing Structure, Channel Coding and Modulation Systems for Broadcasting, Interactive Services, News Gathering and Other Broadband Satellite Applications, part 2: S2-extensions (DVB-S2X)," 2014. [Online]. Available: https://www.etsi.org/deliver/etsi_en/302300_302399/30230702/01.02.01_60/en_30230702v010201p.pdf

[28] L. Lei, L. You, Y. Yang, D. Yuan, S. Chatzinotas, and B. Ottersten, "Load coupling and energy optimization in multi-cell and multi-carrier NOMA networks," *IEEE Trans. Veh. Technol.*, vol. 68, no. 11, pp. 11 323–11 337, Nov. 2019.

[29] A. Celik, M.-C. Tsai, R. M. Radaydeh, F. S. Al-Qahtani, and M.-S. Alouini, "Distributed cluster formation and power-bandwidth allocation for imperfect NOMA in DL-HetNets," *IEEE Trans. Commun.*, vol. 67, no. 2, pp. 1677–1692, Feb. 2019.

[30] M. Kobayashi, J. Boutros, and G. Caire, "Successive interference cancellation with SISO decoding and EM channel estimation," *IEEE J. Sel. Areas Commun.*, vol. 19, no. 8, pp. 1450–1460, Aug. 2001.

[31] R. Fa and R. C. De Lamare, "Multi-branch successive interference cancellation for MIMO spatial multiplexing systems: Design, analysis and adaptive implementation," *IET Commun.*, vol. 5, no. 4, pp. 484–494, 2011.

[32] A. Destounis and A. D. Panagopoulos, "Dynamic power allocation for broadband multi-beam satellite communication networks," *IEEE Commun. Lett.*, vol. 15, no. 4, pp. 380–382, Apr. 2011.

[33] C. W. Tan *et al.* "Wireless network optimization by perron-frobenius theory," *Foundations Trends Netw.*, vol. 9, no. 2-3, pp. 107–218, 2015.

[34] Y. Huang, C. W. Tan, and B. D. Rao, "Joint beamforming and power control in coordinated multicell: Max-min duality, effective network and large system transition," *IEEE Trans. Wireless Commun.*, vol. 12, no. 6, pp. 2730–2742, Jun. 2013.

[35] L. Zheng, D. W. Cai, and C. W. Tan, "Max-min fairness rate control in wireless networks: Optimality and algorithms by perron-frobenius theory," *IEEE Trans. Mobile Comput.*, vol. 17, no. 1, pp. 127–140, Jan. 2018.

[36] Y. Sun, D. W. K. Ng, and R. Schober, "Optimal resource allocation for multicarrier MISO-NOMA systems," in *Proc. IEEE Int. Conf. Commun.*, 2017, pp. 1–7.

[37] C. A. Shaffer, *Practical Introduction to Data Structures and Algorithm Analysis*. Prentice Hall Upper: NJ, USA: Saddle River, NJ, 1997.

[38] K. Sikorski, "Optimal solution of nonlinear equations," *J. Complex.*, vol. 1, no. 2, pp. 197–209, 1985.

[39] S. Boyd and L. Vandenberghe, *Convex Optimization*. Cambridge, U.K.: Cambridge University Press, 2004.

[40] M. Köppe, *On the Complexity of Nonlinear Mixed-Integer Optimization, in Mixed Integer Nonlinear Programming*. Berlin, Germany: Springer, 2012, pp. 533–557.

[41] Q.-D. Vu, K.-G. Nguyen, and M. Juntti, "Weighted max-min fairness for C-RAN multicasting under limited fronthaul constraints," *IEEE Trans. Commun.*, vol. 66, no. 4, pp. 1534–1548, Apr. 2018.

[42] S. P. Schurr, D. P. O'Leary, and A. L. Tits, "A polynomial-time interior-point method for conic optimization, with inexact barrier evaluations," *SIAM J. Optim.*, vol. 20, no. 1, pp. 548–571, 2009.

[43] ESA, SATellite Network of EXperts (SATNEX) IV," [Online]. Available: https://satnex4.org/

[44] D. Zhai, R. Zhang, L. Cai, and F. R. Yu, "Delay minimization for massive internet of things with non-orthogonal multiple access," *IEEE J. Sel. Topics Signal Process.*, vol. 13, no. 3, pp. 553–566, Jun. 2019.

[45] J. P. Choi and V. W. Chan, "Optimum power and beam allocation based on traffic demands and channel conditions over satellite downlinks," *IEEE Trans. Wireless Commun.*, vol. 4, no. 6, pp. 2983–2993, Nov. 2005.

[46] ITU, Time series synthesis of tropospheric impairments, Recommendation ITU-R p.1853-2, Aug. 2019. [Online]. Available: https://www.itu.int/dms_pubrec/itu-r/rec/p/R-REC-P.1853-2-201908-I!!PDF-E.pdf

[47] L. Zheng, Y.-W. P. Hong, C. W. Tan, C.-L. Hsieh, and C.-H. Lee, "Wireless max-min utility fairness with general monotonic constraints by perron-frobenius theory," *IEEE Trans. Inf. Theory*, vol. 62, no. 12, pp. 7283–7298, Dec. 2016.

Anyue Wang (Graduate Student Member, IEEE) received the bachelor's and master's degrees in communication engineering from the Beijing University of Posts and Telecommunications (BUPT), Beijing, China, in 2015 and 2018, respectively. He is currently working toward the Ph.D. degree with Interdisciplinary Center for Security, Reliability and Trust, University of Luxembourg, Luxembourg. His research interests include optimization and machine learning for resource management in wireless communication systems.

Lei Lei (Member, IEEE) received the B.Eng. and M.Eng. degrees from Northwestern Polytechnic University, Xi'an, China, in 2008 and 2011, respectively, and the Ph.D. degree from the Department of Science and Technology, Linköping University, Sweden, in 2016. He is currently a Research Scientist with Interdisciplinary Centre for Security, Reliability and Trust (SnT), University of Luxembourg, Luxembourg. In November 2016, he joined as a Research Associate with SnT, and from June to December 2013, he was a Research Assistant with Institute for Infocomm Research (I2R), A*STAR, Singapore. His current research interests include resource allocation and optimization in 5G satellite networks, energy-efficient communications, and deep learning in wireless communications. He was the recipient of the IEEE Sweden Vehicular Technology-Communications-Information Theory (VT-COM-IT) Joint Chapter Best Student Journal Paper Award in 2014. He was the corecipient of the IEEE SigTelCom 2019 Best Paper Award.

Eva Lagunas (Senior Member, IEEE) received the M.Sc. and Ph.D. degrees in telecommunications engineering from the Polytechnic University of Catalonia (UPC), Barcelona, Spain, in 2010 and 2014, respectively. From 2009 to 2013, she was a Research Assistant with the Department of Signal Theory and Communications, UPC. During the summer of 2009, she was a Guest Research Assistant with the Department of Information Engineering, Pisa, Italy. From November 2011 to May 2012, she held a Visiting Research appointment wiht Center for Advanced Communications , Villanova University, PA, USA. In 2014, she joined the Interdisciplinary Centre for Security, Reliability and Trust (SnT), University of Luxembourg, Luxembourg, where she currently holds a Research Scientist position. Her research interests include radio resource management and general wireless networks optimization.

Ana I. Pérez-Neira (Fellow, IEEE) is a Full Professor with Signal Theory and Communication Department, Universitat Politcnica de Catalunya since 2006, and was the Vice Rector for Research from 2010to 2014. She is a Fellow Researcher with the Centre Tecnologic de Telecomunicacions de Catalunya, where she is the Scientific Coordinator and responsible for the SatCom activities. She has more than 60 journal papers and 300 conference papers. She is the coauthor of seven books, leaded more than 20 projects, and holds eight patents. Her research focuses on signal processing for satellite communications. She is a Coordinator of the Networks of Excellence on satellite communications, financed by the European Space Agency: SatnexIV-V. She is an Associate Editor for the IEEE TRANSACTIONS ON SIGNAL PROCESSING, *the European Association for Signal Processing,* and *American Scientific Publishers*. She is currently the Senior Area Editor of the IEEE OPEN JOURNAL OF SIGNAL PROCESSING. She is a Member of the BoG of the IEEE

Signal Processing Society and the Vice-President for conferences from 2021 to 2023. She is an IEEE Fellow and a Member of the Real Academy of Science and Arts of Barcelona (RACAB). She is the recipient of the 2018 EURASIP Society Award, and she has been the General Chair of the IEEE International Conference on Communications, Signal Processing and their Applications (ICCSPA20, the first big IEEE virtual conference held by the IEEE with more than 15000 attendees.

Symeon Chatzinotas (Senior Member, IEEE) received the M.Eng. degree in telecommunications from the Aristotle University of Thessaloniki, Thessaloniki, Greece, in 2003, and the M.Sc. and Ph.D. degrees in electronic engineering from the University of Surrey, Surrey, U.K., in 2006 and 2009, respectively. He is currently a Full Professor and Chief Scientist I, and the Co-Head of the SIGCOM Research Group, Interdisciplinary Center for Security, Reliability and Trust, University of Luxembourg, Luxembourg. He was a Visiting Professor with the University of Parma, Parma, Italy, and he was involved in numerous research and development projects for the National Center for Scientific Research Demokritos, the Center of Research and Technology Hellas, and the Center of Communication Systems Research, University of Surrey. He has coauthored more than 400 technical papers in refereed international journals, conferences, and scientific books. He was the corecipient of the 2014 IEEE Distinguished Contributions to Satellite Communications Award, the CROWNCOM2015 Best Paper Award, and the 2018 EURASIP JWCN Best Paper Award. He is currently on the Editorial Board of the IEEE OPEN JOURNAL OF VEHICULAR TECHNOLOGY and the *International Journal of Satellite Communications and Networking*.

Björn Ottersten (Fellow, IEEE) was born in Stockholm, Sweden, in 1961. He received the M.S. degree in electrical engineering and applied physics from Linköping University, Linköping, Sweden, in 1986 and the Ph.D. degree in electrical engineering from Stanford University, Stanford, CA, USA, in 1990. He has held research positions with the Department of Electrical Engineering, Linköping University, the Information Systems Laboratory, Stanford University, the Katholieke Universiteit Leuven, Leuven, Belgium, and the University of Luxembourg, Luxembourg. From 1996 to 1997, he was the Director of Research with ArrayComm, Inc., a start-up in San Jose, CA, USA, based on his patented technology. In 1991, he was appointed as a Professor of signal processing with the Royal Institute of Technology (KTH), Stockholm, Sweden. From 1992 to 2004, he was the Head of the Department for Signals, Sensors, and Systems, KTH, and from 2004 to 2008, he was the Dean of the School of Electrical Engineering, KTH. He is currently the Director for the Interdisciplinary Centre for Security, Reliability and Trust, University of Luxembourg. As Digital Champion of Luxembourg, he acts as an Adviser to the European Commission. He was the recipient of the IEEE Signal Processing Society Technical Achievement Award in 2011 and the European Research Council advanced research grant twice, in 2009–2013 and in 2017–2022. He has coauthored journal papers that received the IEEE Signal Processing Society Best Paper Award in 1993, 2001, 2006, and 2013, respectively, and seven other IEEE conference papers Best Paper Awards. He was the Editor-in-Chief of the EURASIP *Signal Processing Journal*, an Associate Editor for the IEEE TRANSACTIONS ON SIGNAL PROCESSING, and the Editorial Board of the IEEE Signal Processing Magazine. He is currently a Member of the Editorial Boards of the EURASIP *Journal of Advances Signal Processing* and *Foundations and Trends of Signal Processing*. He is a Fellow EURASIP.